FLORIDA STATE UNIVERSITY

COLLEGE OF ARTS AND SCIENCES

U-PB ISOTOPIC DATING OF THE PITCHBLENDE ORE MINERALIZATION AT THE COLES HILL, PITTSYLVANIA, VIRGINIA, USA

By

LAUREN R. OLSEN

A Thesis submitted to the
Department of Earth, Ocean, and Atmospheric Science
in partial fulfillment of the
requirements for the degree of
Master of Science

2016

Lauren Olsen defended this thesis on April 7, 2016.

The members of the supervisory committee were:

A. Leroy Odom

Professor Directing Thesis

James F. Tull

Committee Member

Stephen A. Kish

Committee Member

The Graduate School has verified and approved the above-named committee members, and certifies that the thesis has been approved in accordance with university requirements.

To all my family

ACKNOWLEDGMENTS

I would like to show my appreciation by giving a heartfelt thank you to all those whom provided me with their suggestions, support, and encouragements throughout my time spent at Florida State University. I feel honored to have learned from and worked with many geoscientists from the Department of Earth Ocean Atmospheric Sciences (EOAS), Department of Geology, the National High Fields Magnetic Library (NHFML) Geochemistry Department, the Virginia's Museum of Natural History, and Virginia Uranium. These professors and geoscientists provided me with the wealth of information and knowledge required to pursue and complete a Master's degree in Geology.

I would like to thank my thesis committee members, faculty, and staff at Florida State University for all of their help and guidance the past three years. I could not have completed this without my advisor Dr. Leroy Odom. He has been a mentor for me since I first voiced my decision to pursue a M.S. degree at Florida State University. I want to thank him for suggesting the idea for my thesis project, accompanying me to my field work, and providing the knowledge and skill set to complete it. He generously provided a means of scholarship as a teaching assistant, and continues to inspire me to pursue a career in the mining industry. I will always admire how knowledgeable Dr. Odom is about geochemistry, and one day hope to be a successful geoscientist like him.

I'd like to show my appreciation to Dr. James Tull and Dr. Stephen Kish for their elite knowledge of the geosciences throughout my years as a student, and for serving on my thesis committee. Thank you to both for the suggestions on my thesis and input throughout the years. Thank you to Dr. James Tull for his support and encouragement to pursue a geology Master's degree at FSU, and his extensive knowledge about structural geology in the Appalachian Mountains. Thank you to Dr. Stephen Kish for his wealth of knowledge of ore deposit geology, geochemistry, as well as his research experience in Appalachians.

A special thank you to both Jim Beard of Virginia's Museum of Natural History and Joe Aylor of Virginia Uranium for their generosity and communications regarding my thesis project. I want to thank Joe Aylor owner of Virginia Uranium Corporation for allowing me to collect samples from Coles Hill, and taking the time to show Dr. Odom and I around the deposit and surrounding outcrops. I want to thank Jim Beard head geologist at the Virginia Museum of

Natural History for taking the time to discuss the Coles Hill deposits in detail with us, and providing an electron backscatter image for my research.

I have been able to work with the scientific staff at National High Fields Magnet Laboratory's Department of Geochemistry. A special thank you to Dr. Vincent Salters and Afi Sachi-Kocher for their instruction and guidance while working on my research. A special thank you to Afi Sachi-Kocher for assisting with the chemistry of samples in the clean laboratory. Also a special thank you to Dr. Vincent Salters and Gary White for taking the time to set up and monitor the use of the Neptune and Element 2 instruments while running my samples.

I am beyond thankful for all of my family, for their continuous supporting my goals to further my education, and reminding me that I will fulfill my dreams. Words can't describe how thankful I am to have my mother and nana who have always believed in my determination to become a geologist. I will never forget my nana always telling me to "finish school first." I am blessed to have my family's unconditional love and support as I finish my master's degree. My family has taught me to do all things with confidence, work hard at it, and to never give up on your dreams, and with that dedicate my success in the geologic sciences to them.

TABLE OF CONTENTS

List of Tables vii
List of Figures viii
Abstract ix

CHAPTER 1 INTRODUCTION 1

1.1 Geologic Setting of the Coles Hill Uranium Deposit 1
1.2 Smith River Allochthon Lithology 2
1.3 Structural Deformation 5
1.4 Metamorphism 8
1.5 Uranium Deposit Types 9
1.6 Uranium Examples 12
1.7 Coles Hill Uranium Deposit 16
1.8 Current Research 20

CHAPTER 2 U-PB SYSTEMATICS 27

2.1 U-Pb Geochronology, Uranium Lead Ratio Systematics 27

CHAPTER 3 METHODS 35

3.1 Sampling 35
3.2 Analytical Procedure 35

CHAPTER 4 RESULTS 38

4.1 Data Results 38

CHAPTER 5 DISCUSSION 45

5.1 Coles Hill Uranium Deposit 45

References 48

Biographical Sketch 55

LIST OF TABLES

3.1 Pb Column Worksheet, provided by Afi Sachi-Kocher.....37

4.1 Sample data from the Element 2 and Neptune measurements.....40

LIST OF FIGURES

1.1 Coles Hill regional geologic map and cross section of ore bodies (From Jerden, 2001) 22

1.2 Geologic map of Coles Hill site lithological units, and exploration drill hole locations of the south ore body (Marline Corporation, 1983). 23

1.3 Conceptual model for the formation of the Coles Hill uranium deposit (Jerden, 2001) 24

1.4 Geologic cross-section X-X' of Coles Hill uranium deposit host rocks constructed from Marline Corporation exploration drill hole data. (From Jerden, 2001; Marline Corporation, 1983). 25

1.5 Coles Hill deposit, (a) plan view of surface projected ore bodies and (b) S-N outlined by cutoff grade of 0.084% U (Dahlkamp, 2010; After Maxwell et al., 2008).....26

2.1 Pb*/U Concordia diagram, showing the three chronometers that are commonly used (Gehrels, 2012) 32

2.2 Diagram showing that, for a mid-Proterozoic analysis with Pb loss, the $^{206}Pb^*/^{207}Pb$ age is more accurate than $^{206}Pb^*/^{238}U$ and $^{207}Pb^*/^{235}U$ ages (Gehrels, 2012).....33

2.3 Shows the trajectory of a line above Concordia that is representative of U-loss within the system (Adapted from Gehrels, 2012) 34

4.1 U/Pb Isochron shows discordance between samples from Coles Hill.....41

4.2 U-Pb Concordia plot for the most radiogenic samples corrected for common Pb values 42

4.3 Concordia samples with the highest radiogenic values plot above concordia.....43

4.4 Pb/Pb Isochron is a plot of the least radiogenic samples corrected for common Pb values....44

5.1 Electron Backscatter Image of the UO_2 with micron size galena (personal communication Beard, 2015).....47

ABSTRACT

The study conducted U-Pb isotopic dating of the pitchblende mineralization of the Coles Hill uranium deposit in Pittsylvania County, VA. The ore body is found along the Chatham fault and within the Martinsville Igneous Complex. In attempt to constrain the time of uranium mineralization, samples were collected within the fractures to the west of the Chatham fault that separates the host rock from the Danville Basin. Fifteen samples were analyzed for uranium and lead concentrations, as well as their isotopic lead compositions.

BSE imaging revealed that the milligram sized samples consisted of multiple phases mixed on a micron scale. Uranium and lead isotopic analyses revealed that some phase or phases contained highly radiogenic ($^{206}Pb/^{204}Pb$ ratios between 2,000 and 3,000) while some phases or phases were dominated by common lead.

Highly discordant Pb/U ages of the highly radiogenic samples seem to be due to recent loss of substantial amounts of uranium. Analyses of these on a Concordia plot seems to indicate that uranium loss was not in a single event but occurred over time and likely recently. Therefore it was not possible to directly determine the age of the uranium mineralization.

The four samples dominated by lead lie closely at 1115 Ma Pb-Pb isochron. It is inferred from this that the common lead present was derived from Grenville age basement that underlies the Smith River Allochthon.

CHAPTER 1

INTRODUCTION

1.1 Geologic Setting of the Coles Hill Uranium Deposit

The Coles Hill uranium deposit of Pittsylvania County, Virginia (Fig. 1.1) was discovered with a gamma ray scintillation counter by Marline Uranium Inc. in 1978. The ore deposit consists of two structurally controlled, hydrothermal ore bodies (designated as North and South ore bodies) hosted in igneous cataclastic zones along the northwest margin of the Danville Triassic Basin (Jerden, 2001) and within the Martinsville Igneous Complex. The Martinsville Igneous complex forms the footwall of the Danville Basin border fault (Chatham Fault) (Fig. 1.2 and 1.3), and is composed of the Leatherwood granite and Rich Acres gabbro which intrudes part of the Fork Mountain Formation of Late Ordovician to Silurian age.

The region is within the western Piedmont's Smith River allocthon (Conley and Henika 1973; Hibbard, et al. 2003). The major rock types of the Smith River allocthon in the vicinity of Coles Hill are Fork Mountain Formation, Leatherwood granite, and Rich Acres Igneous suite (Henika, 1998; Aylor et al., 2014).The Leatherwood granite is considered to be a high-K, calc-alkaline series rock (Hibbard et al., 2014) and is thought to be intruded by the Rich Acres gabbro (Aylor et al., 2014). The hanging wall to the east of the Chatham fault includes Triassic metasedimentary rocks such as, the Fork Mountain mica schist, Chatham fault unconsolidated sand, and Triassic cataclasite are not recognized in outcrop but are present in the drill core (Aylor et al., 2014). From previous work on core site by Aylor et al. (2011), an open fold pattern with fold axis perpendicular (Conley and Henika, 1973; Conley, 1985) to the Chatham fault has been identified—fold axes strike 030° 60°SE (Aylor et al., 2014).

The Chatham fault (Myertons, 1963) bounds the northwestern part of the Danville Triassic basin (Conley, 1985). It truncates the Ridgeway fault in the south-central part of the area and from there northeastward forms the northwestern boundary of the Smith River allochthon (Conley, 1985). Farther northeastward the fault strikes approximately N50°E, which is its trend direction through the rest of the area to the north (Conley, 1985). The fault dips 60° to 70° south or southeast (Conley, 1985).

1.2 Smith River Allochthon Lithology

The Smith River Allochthon (SRA) is a large synform that overlies Lynchburg Group and Grenville-age basement rocks (Henika et al., 1996). The lithology of the SRA is comprised of the Basset Formation, Fork Mountain Formation, and the Martinsville Igneous Complex (MIC). The allochthonous rocks include a metavolcanic and metasedimentary sequence of Late Precambrian to Early Paleozoic age intruded by the Cambro-Ordovician MIC (Henika et al., 1996). According to Conley and Henika (1973) three episodes of metamorphisms are believed to have effected this area: 1) Barrovian-type regional metamorphism, 2) a later retrograde event, 3) contact metamorphism due to the igneous plutons (Henika et al., 1996).

1.2.1 Basset Formation

The Basset Formation is exposed within the cores of a series of domes within the SRA (Henika et al., 1996). It is composed of two metasedimentary-volcaniclastic lithofacies, a massive to layered granitic gneiss unit overlain by or interlayered with a banded amphibolite unit (Henika et al., 1996). The formation is cut by numerous quartz-feldspar and mica-quartz-feldspar dikes and sills in areas surrounding the MIC (Henika et al., 1996).

1.2.2 Fork Mountain Formation

The Fork Mountain Formation overlies the Basset formation and is composed of a mica schist and a biotite gneiss. Mica schist is predominant in the upper part of the formation, and underlies northeastward-trending ridges along the north western edge of the allochthon whereas the biotite gneiss is predominant to the south east in the Martinsville area adjacent to or directly overlying the MIC (Henika et al., 1996).

1.2.2.1 Mica Schist. The schist is composed primarily of muscovite, biotite, quartz, garnet, and chlorite with accessory amounts of plagioclase, epidote, clinozoisite, magnetite, and titanium bearing minerals (Henika et al., 1996). Chloritoid, staurolite, kyanite, and sillimanite porphyroblasts all show complex prograde and retrograde paragenesis (Conley and Henika, 1973; Conley, 1985; Henika et al., 1996). Andalusite has been recently confirmed in Fork Mountain schist by X-ray microprobe studies of poikiloblasts in the early-formed staurolite grade regional metamorphic assemblage zone (Henika et al., 1996). The mineral assemblage indicates

that conditions of metamorphism reached 520 to 575 degrees C and 2 to 3.5 kb pressure (Henika et al., 1996). The staurolite crystals that formed during regional metamorphism northwest of the staurolite-sillimanite isograd (Henika, 1971; Conley, 1985) are large (1-7 cm), typically amber in color, generally twinned and partially to totally altered to sericite pseudomorphs ("fairystones") (Henika et al., 1996). Biotite occurs in the mica schist, but to the southeast of the relict sillimanite isograd it is almost universally altered to chlorite (Henika et al., 1996). Masses of fibrolite, partially altered to sericite, are diagnostic of the rocks southeast of the relict sillimanite isograd (Henika et al., 1996). Some of this sillimanite is pseudomorphous after staurolite and contains poikiloblastic inclusions of quartz and garnet (Henika et al., 1996).

1.2.2.2 Biotite Gneiss. The Fork Mountain biotite gneiss is a medium-gray, compositionally banded rock consisting of quartzo-feldspathic layers and garnetiferous muscovite-biotite layers (Henika et al., 1996). The gneiss contains about equal amounts of quartz (commonly bright blue) and plagioclase and varying amounts of biotite, microcline, garnet, muscovite, and kyanite sillimanite (Henika et al., 1996). Opaque minerals, garnet, and kyanite-sillimanite occur primarily in the biotite-rich layers; whereas, the quartzo-feldspathic layers are composed predominantly of quartz, plagioclase, microcline, and minor amounts of biotite and muscovite (Henika et al., 1996). Metamorphosed matrix- supported lithic breccias composed of gneiss, quartzite and amphibolite clasts up to 45 cm across are characteristic of the Fork Mountain biotite gneiss (Henika et al., 1996).

1.2.3 Martinsville Igneous Complex (MIC)

The Martinsville Igneous Complex (Ragland, 1974) is composed of two separate plutonic units: the Leatherwood Granite (Jonas, 1928) and the Rich Acres Igneous Suite (Conley, 1985; Conley and Henika, 1973; Henika et al., 1996). The igneous complex underlies a large area around Martinsville; isolated plutons also occur to the east of the main outcrop area (Henika et al., 1996). Radiometric dates from the Leatherwood Granite (U/Pb, zircons, and Rb/Sr whole-rock analyses) show that it is either Middle Ordovician in age (450 Ma, Rankin, 1975; 464 + 20 Ma, Odom and Russell, 1975) or Cambrian in age (516 Ma, Sinha et al., 1989; Henika et al., 1996).

1.2.3.1 Rich Acres. The Rich Acres Igneous Suite makes up the major part of the Martinsville Igneous Complex. It generally occurs in concordant to slightly discordant plutons, intrudes into the Fork Mountain and Bassett Formations (Henika et al., 1996). The composition of the Rich Acres ranges from syenodiorite to norite; however the suite is dominantly diorite (Henika et al., 1996).

The syenodiorite and gabbro are commonly dark-greenish-gray, medium-grained rocks that have ophitic to subophitic textures (Henika et al., 1996). These plutonic rocks are composed of the minerals plagioclase, green hornblende, reddish-brown biotite, pale-green clinopyroxene, uralite, and quartz as vermicular intergrowths in hornblende and plagioclase (Henika et al., 1996). The outer parts of some plutons are injected with thin hornblende diorite or hornblende gabbro dikes and quartz-microcline-oligoclase pegmatites (Henika et al., 1996).

The norite dikes are small with dark-gray, porphyritic to ophitic-textured. The rock is composed of plagioclase (bytownite-labradorite), orthopyroxene (predominantly hypersthene), clinopyroxene, brown pargasite, brown biotite, green hornblende (uralite), and olivine (Henika, et al., 1996).

Ultramafic bodies are conformable within surrounding geology of the Rich Acres Igneous Suite, and are highly deformed and folded along the southeastern boundary of the MIC (Henika et al., 1996). According to Henika and others (1996) the sills are several hundred feet thick and up to six miles long. They have two predominant lithologies: light green to light gray talc schist and dark greenish gray granular rock. A thin section from the schist body contains approximately 35 percent cummingtonite, 20 percent talc, 10 percent chlorite, and 5 percent opaque minerals (Conley and Henika, 1973; Henika et al., 1996). Both lithologies may occur in the same body and intergrade with each other (Henika et al., 1996).

Areas underlain by rocks in the Rich Acres Igneous Suite are generally lowlands that have a gentle rolling topography (Henika et al., 1996). Where the soil profile is preserved, Rich Acres soils are commonly distinguished by a surface gravel of dark-brown iron oxide concretions in the topsoil layers (Henika et al., 1996). Thick, dark-brown iron oxide dusty-red, high-shrink-swell clay soils overlie the structureless saprolite (Henika et al., 1996).

1.2.3.2 Leatherwood Granite. The Leatherwood granite occurs as dikes, sill-like bodies, and irregularly-shaped plutons (Henika et al., 1996). The major part of the Leatherwood occurs as thin sheets on top of the large plutons of Rich Acres (Henika et al., 1996). The post-metamorphic Leatherwood granite has a Rb-Sr whole rock age of 462 ± 20 Ma (Odom and Russell, 1975). The Leatherwood is medium-grained to coarse-porphyritic, light-gray granite that generally shows rapakivi texture (Henika et al., 1996). However, sheets of fine-to coarse-grained equigranular, leucocratic granite and alaskite are exposed in some of the larger Rich Acres plutons (Henika et al., 1996). Some specimens of the granite contain oligoclase as well as microcline phenocrysts, the phenocrysts are set in a medium-grained xenomorphic-granular matrix composed of microcline, quartz, plagioclase, biotite, and muscovite (Henika et al., 1996).

The granite locally exhibits mylonitic textures (Henika et al., 1996). Large quartz grains occur as unstrained, recrystallized polygonal aggregates that show well defined decussate growth (Henika et al., 1996). Microcline phenocrysts are rimmed by fine grained, recrystallized quartz and feldspar that has been shown experimentally to indicate ductile deformation at temperatures above 700 degrees C (Tullis and Lund, 1987; Henika et al., 1996).

The Leatherwood weathers to a pinkish, granular saprolite and brown to yellowish-red, well-drained, gravelly, sandy soil (Henika et al., 1996). It is expressed topographically as low convex hills and v-shaped valleys (Henika et al., 1996). Bedrock is not commonly exposed on the upland surface but large boulders and granite pavements are commonly developed along the v-shaped valleys (Henika et al., 1996).

1.3 Structural Deformation

According to Aylor et al. (2014) “the rocks have been modified by up to as many as four deformational events and by metamorphic events, including the Taconic, Acadian, Alleghanian, orogenies and again during the Mesozoic rifting.” The geologic history of early Paleozoic tectonics may relate this region to subduction related arc magmatism associated with the closure of the Iapetus Ocean and Taconic Orogeny. The Triassic Danville Basin to the east of the Chatham fault (Mesozoic) boundary may relate with extensional tectonics as the arc matured.

1.3.1 Smith River Allochthon Anticlinorium

The Smith River allochthon is preserved in a long northeast-trending, synformal structure located between the Blue Ridge anticlinorium and the Sauratown Mountains anticlinorium (Conley and Henika 1973; Conley, 1985; Henika et al., 1996). Upright northeast trending antiforms and synforms involving the Fork Mountain and Bassett Formations along the northwest side of the allochthon (Henika, 1971) belong to northeastward-trending (F_2 and F_3) fold systems that modify recumbant (F_1) isoclinal folds in the central part of the allochthon (Henika, et al., 1996). The major F_2, folds in the allochthon are long and narrow structures with gently plunging hinges to the south, some of which can be traced for tens of miles between abrupt culminations (Henika et al., 1996). F_3 folds in the allochthon are shorter, more open, and more steeply southwest plunging folds than the earlier structures (Henika et al., 1996). The F_3 fold hinges have more northerly trends at acute angles to major formational boundaries indicating a dextral shear symmetry (Gates, 1986; Henika et al., 1996). The F_3 folds produce hook-shaped interference patterns where they cross the F_2 folds.

Nappe-like F_1 isoclinal folds occur within the allochthon (Henika, 1971) have subhorizontal axial planes (Henika et al., 1996). Henika and others (1996) suggest that these structures were probably formed during Taconic or Pre-Taconic collisional tectonism and Barrovian regional metamorphism dated at 534 Ma by Gates and others (1994) suggests earlier formation during the Neoproterozoic. Later sets of more upright folds (F_2 and F_3) have refolded the subhorizontal folds in type 2 interference (Ramsey, 1967) and deformed the regional metamorphic rock fabrics in the allochthon (Henika, 1971; Conley and Henika 1973; Ramsey, 1967; Henika et al., 1996).

The syncline that preserved the allochthon was probably produced during the initial stages of Alleghanian thrusting (F_2) (Henika et al., 1996). The relict isogradic boundary between the mica schist and biotite gneiss units of the Fork Mountain Formation (Henika, 1971) probably deformed by dextral shearing along the Bowens Creek fault during a later (F_3) phase of tectonism that was coincident with the late Paleozoic (350 to 275 Ma Rb/ Sr whole rock and mineral) ages reported from rocks along the Bowens Creek fault (Gates, 1986; Fullagar and Deitrich, 1976; Henika et al., 1996).

1.3.2 Danville Basin

The Mesozoic basin is bounded on its northwestern margin by the Chatham fault (Myertons, 1963; Henika et al., 1996). The sedimentary rocks on the southeastern margin of the basin may be either in unconformable or fault contact with the older metamorphic rocks (Myertons, 1963; Henika et al., 1996). Strike of bedding within the basin generally is parallel to the trend of the Chatham fault zone and the rocks have a rather consistent north 44 degrees west dip, except near the Chatham fault, where the dips are steeper (Thayer, *in* Henika, 1977; Henika et al., 1996). The estimated thickness of strata in the Danville basin, calculated from outcrop width and average dips, ranges from 3,600 feet in the narrowest part of the basin to 13,300 feet in the widest part (Henika and Thayer, 1980; Henika et al., 1996).

1.3.3 Chatham Fault

The fault is a northeast trending normal fault along which the (Mesozoic) movement was down to the southeast extension (Henika et al., 1996). The fault zone contains a belt of mylonitic and cataclastic rocks as much as 0.5 mile wide that includes rocks derived from intense shearing of metamorphic rocks located northwest of the Danville basin and Mesozoic-age sedimentary rocks from within the basin (Henika and Thayer, 1977; Price et al., 1980a, 1980b; Henika et al., 1996).

The consistency of trend and dip of the Mesozoic rocks that fill the Danville basin indicates that little movement occurred along the Chatham fault during deposition in the basin (Henika et al., 1996). The latest movement along the Chatham fault postdates deposition of the sedimentary rocks and was down to the east extension that rotated the strata within the basin so that they now have dip angles ranging from 30 to 45 degrees to the northwest (Henika et al., 1996).

The Chatham fault zones may record multiple deformation events. Robinson (1979) reported undeformed pegmatite intruding mylonitic rocks of the Sauratown Mountains anticlinorium along the Chatham fault zone (Henika et al., 1996). The mylonitization corresponds with pegmatite intrusions in the Sauratown Mountains anticlinorium to the southwest that has dated muscovites using the Rb-Sr method at 321 Ma (Deuzer and Herzog, 1962; Henika et al., 1996). This early ductile movement may be associated with the Brookneal

shear zone described by Gates (1981) along strike to the northeast or with the Stoney Ridge branch of the Brevard fault described by Butler and Dunn (1968) along strike to the southwest of the Chatham fault in North Carolina (Henika et al., 1996). Samples of silicified microbreccia characteristic of the later brittle deformation in North Carolina have been dated as the Early Jurassic age (180 ± 3 Ma) by Fullagar and Butler (1980) (Henika et al., 1996).

1.4 Metamorphism

1.4.1 Taconic Metamorphism

The first episode of regional metamorphism of the Smith River terrane is proposed to have occurred during the Taconic Orogeny (Glover et al., 1983; Gates, 1987). The peak of M_1 metamorphisms attained middle to upper amphibolite facies and is characterized by sillimanite and staurolite bearing assemblages (Conley and Henika, 1973; Gates, 1981; Gates, 1987). The Leatherwood granite intrudes the SRA postdating peak metamorphism (Conley and Henika 1973; Conley, 1978) and has been dated at 462 ± 20 Ma old using Rb/Sr whole rock methods (Odom and Russell, 1975; Gates, 1987). Rb/Sr biotite whole-rock ages of 440 ± 22 Ma (Odom and Russell, 1975) obtained from pelitic, sillimanite-staurolite gneisses in the center of the Allochthon (Gates, 1987). The ages indicate that the amphibolite grade M_1 metamorphism is Ordovician in age (Gates, 1987).

1.4.2 Post Taconic Metamorphism

The Martinsville Igneous complex is composed of the Leatherwood granite, and Rich Acres gabbro with amphibolites. The Leatherwood granite, which intrudes gneisses and schists of the Smith River allochthon is 464 ± 20 Ma old (Odom and Russell, 1975). The granite post-dates the regional metamorphism and primary schistosity of rocks of the Smith River Allochthon (Odom and Russell, 1975). Considering the uncertainties of the isochron ages, the Leatherwood Granite could be as young as 444 Ma, while the two gneisses of the Inner Piedmont are younger than 460 Ma (Odom and Russell, 1975). The Smith River and Inner Piedmont allochthons occupy the same structural position within the southern Appalachian orogeny and are separated only by the Sauratown Mountains Anticlinorium (Odom and Russell, 1975). If rocks of both allochthons were progressively metamorphosed at nearly the same time, then the Barrovian

metamorphism occurred very close to 450 Ma ago, Ordovician age intrusions (Odom and Russell, 1975).

1.4.3 MIC Ordovician Intrusions

Near Rich Acres Igneous Suite contacts, the metapelites have recrystallized under static metamorphic conditions causing widespread decussate growth of mica, kyanite, and sillimanite porphyroblasts, especially in sites of large, previously retrograded staurolite or kyanite/sillimanite porphyroblasts (Conley and Henika 1973; Henika et al., 1996). Maximum metamorphic temperature and pressure ranges for rocks from the thermal aureole near Collinsville were estimated by the Virginia Tech Igneous and Metamorphic Petrology Laboratory to be approximately 4 to 8 kb of pressure and 635 to 725 degrees C temperature using a petrogenetic grid (Henika et al., 1996). The rocks of the Fork Mountain Formation, in contact with the Martinsville Igneous Complex commonly contain zones of incipient melting, mica-quartz-microcline migmatite layers, and cross-cutting granitic to granodioritic dikes (Henika et al., 1996). Coarse sillimanite porphyroblasts occur in the migmatite zone (Henika et al., 1996). Away from this zone they are progressively replaced in order by fibrolite sprays, finer-grained kyanite, and microscopic, untwinned staurolite porphyroblasts (Conley and Henika, 1973; Henika et al., 1996).

1.5 Uranium Deposit Types

Uranium ore deposits are associated with different geologic environments. The deposition includes transport, which often indicate the source of hydrothermal fluids, origin of the uranium, and environment for precipitation. They are classified based off of geotectonic position, host rock type, and ore body morphology (Bruneton, 2014).

1.5.1 Hydrothermal Mineralization

Hydrothermal U-ore mineralization occurs when large volumes of warm oxidizing water leach U(VI) (by converting U^{+4} to the uranyl complex ion) from the surrounding source rock into hydrothermal fluids. The uranyl complex precipitates out U(IV) such as pitchblende, in places where the solubility of uranium changes with changing redox conditions (Lehman, 2008).

Geochemical formula: $U^{6+} + 2e^- = U^{4+}$

In a natural system: $UO_2(CO_3)_2^{2-} + H^+ = UO_2 + ½ O_2 + 2CO_2 + H_2O$

This equation describes the solubility as a function of pH buffered by rocks, the solubility of the uranium will be controlled by the concentration of CO_2 and O_2 in solution (Lehman, 2008). Uranium ore formation by precipitation as uraninite from oxidized solutions marks the transition from oxidized to reduced environments (Lehman, 2008).

Three major types of hydrothermal uranium ore deposits provide about 85 percent of the present-day world uranium mine production. These are (1) unconformity-related uranium deposits, (2) sandstone-hosted or roll front deposits, and (3) IOCG (Iron Oxide-Copper-Gold) deposits (Lehman, 2008). All three types form at redox fronts where oxidized basinal brines or meteoric water meet reducing lithologies or methane bearing fluids (Lehman, 2008).

1.5.2 Unconformity Type Deposits

Unconformity related deposits are associated with and occur immediately below and above an unconformable contact that separates a crystalline basement intensively altered from overlying clastic sediments of Proterozoic age (IAEA, 2009).

Unconformity related deposits arise from geological changes occurring close to major Proterozoic unconformities (World Nuclear Association, 2015). Below the unconformity, the metasedimentary rocks which host the mineralization are usually faulted and brecciated (World Nuclear Association, 2015). The overlying younger Proterozoic sandstones are usually undeformed (World Nuclear Association, 2015). Unconformity related deposits constitute about one third of the western world's uranium resources, including the Athabasca Basin in Canada (World Nuclear Association, 2015). Minerals are uraninite and pitchblende associated with strong quartz dissolution (World Nuclear Association, 2015).

1.5.3 Roll Front Deposits

Roll front deposits form due to the migration of groundwater though permeable sandstones and conglomerates. The sandstone related uranium deposits occur in medium- to coarse-grained sandstones deposited in a continental fluvial or marginal marine sedimentary

environment (World Nuclear Association, 2015). Impermeable shale or mudstone units are interbedded in the sedimentary sequence and often occur immediately above and below the mineralized sandstone (World Nuclear Association, 2015). Uranium is precipitated under reducing conditions caused by a variety of reducing agents within the sandstone including: carbonaceous material, sulfides, hydrocarbons, and interbedded volcanic ash with abundant ferromagnesian minerals (World Nuclear Association, 2015). Sandstone hosted or roll-front deposits concentrate U-mineralization in sandstone aquifers where the environment can change from oxidized to reduced conditions (Lehman, 2008). The hydrothermal alteration that preceded U-mineralization transmitted their reduced environment that is seen by the presences of hydrothermal halos into the overlying sandstone (Lehman, 2008). Gangue minerals associated with roll front deposits include pyrite, hematite, quartz, feldspar, calcite, sericite, and chlorite.

The mineralized zones are convex down the hydrologic gradient (IAEA, 2009). They display diffuse boundaries with reduced sandstone on the down-gradient side and sharp contacts with oxidized sandstone on the up-gradient side (IAEA, 2009). The mineralized zones are elongate and sinuous approximately parallel to the strike, and perpendicular to the direction of deposition and groundwater flow (IAEA, 2009).

1.5.4 Vein Type deposits

Vein type deposits are related to intrusive deposits, granite related deposits, and poly metallic iron oxide breccia complex deposits (IOCG). They are formed by filling an open fissure or fracture within a rock (IAEA, 2009). In vein deposits, the major part of the mineralization fills fractures with highly variable thickness, and generally important extension along strike (IAEA, 2009). The veins consist mainly of gangue material and ore material is mainly pitchblende (IAEA, 2009). Gangue minerals commonly associated with vein deposits are magnetite, hematite, quartz, and calcite.

Uranium bearing veins are present in crystalline rocks, like Coles Hill. Veins and shear-zone deposits are related to fold- and thrust-belts, produce U from black shales (phosphate), and higher U concentrations at a synsedimentary redox front that was further upgraded by weathering (Lehman, 2008). High temperature vein intrusions and shear zones alter the region by metasomatic albitization, followed by chloritization, and U-ore mineralization.

1.5.4.1 Intrusive & Granite Related Deposits. Intrusive and granite related deposits form during the final stages of magma crystallization. As an intrusive body cools the hydrothermal fluids exsolve into fractures within the pluton and in the surrounding country rock. Thermal gradients produced by contact metamorphism then drive the mineralizing fluids into the surrounding rocks. These hydrothermal fluids can then circulate within these systems leaching uranium from the pluton and county rocks and precipitate ore minerals within fractures.

Included in this type are those associated with a variety of intrusive rocks including alaskite, granite, pegmatite, and monzonites (World Nuclear Association, 2015). Intrusive sub-types include anatectic or pegmatites/alaskites, and plutonic granite-monozites/porphyry copper. Intrusive uranium types typically produce U ore as a byproduct of Cu-Au-Mo, TREE, Nb-Ta-Zr, P, Th and are related to magmatic differentiation (Bruneton, 2014).

Granitic related deposits include many vein deposits in granite, deposits in adjacent meta-sedimentary rocks, and also disseminated mineralization in the granite (World Nuclear Association, 2015). Two sub-types include endogranitic and perigranitic with veins-stockwork or disseminated mineralization into granite internal episyenite bodies that are often gradational to veins (Bruneton, 2014).

1.5.4.2 Poly Metallic Iron Oxide Breccia Complex. These types occur in a hematite rich granite breccia complex and contain uranium in association with copper, gold, silver, and rare earths (Bruneton, 2014). Referred to as Iron-Oxide-Copper-Gold systems (IOCG) or IOCGU when enriched with uranium. The Olympic Dam in Australia is the largest explored deposits of this type.

1.6 Uranium Examples

Uranium deposits do not have a restricted set of formulated conditions for deposition. Deposits often have similarities or differences based on the type of transport of uranium and deposition conditions. Similarities between textures and metasomatic alterations can be seen by the mineralization that is present. Examples such as the Athabasca basin deposit, the Schwartzwalder deposit, and the Olympic Dam deposit, may present similar means of deposition like that found at Coles Hill.

1.6.1 Athabasca Basin, Unconformity Type

Unconformity deposits of the Athabasca Basin are the world's largest storehouse of high-grade uranium resources and are the sole producers of Canada's primary uranium (Jefferson et al., 2007). The uranium ore deposits are pods, veins, and semi-massive replacements consisting of mainly uraninite dated between 1600 to 1350 Ma, and located close to basal unconformities between Proterozoic red bed basins and metamorphosed basement rocks, especially supracrustal gneiss with graphitic metapelite (Jefferson et al., 2007). The basin has been subjected to tectonically active orogenic and ductile shear zones during periods of convergence (Jefferson et al., 2007). The polymetallic deposits, commonly subhorizontal ore lenses straddle the unconformity, replacing sandstone and altered basement rock with variable amounts of U, Ni, Co, and As, and traces of Au, PGEs, Cu, REEs, and Fe (Jefferson et al., 2007). High heat flow could have resulted from the voluminous high-U granitoid intrusions within these orogens (Jefferson et al., 2007).

Paleo-weathering, fluid migration, and fault structures may have influenced the migration of U. The U-enriched basement granites and pegmatites, also rich in K, Th, and rare earth elements (REE), may have selectively contributed U to the overlying basins through a variety of mechanisms (Jefferson et al., 2007). Mechanisms include the reactivation of faults offset by unconformities, interactions between graphite metapelite gneiss, quartz-dominated U depleted strata, and large scale hydrothermal alterations. The graphitic metapelitic gneiss units are not only conductive targets and the sites of reactivated faults, but are also speculated as a key source of reductant in geochemical process models for unconformity-associated U (Jefferson et al., 2007; Hoeve and Sibbald, 1978; McCready et al., 1999; Wilson et al., 2007). Graphitic units may also have focused U precipitation from hydrothermal fluids by conducting deep heat sources to drive convection (Hoeve and Quirt, 1984) or by serving as anodes of natural electrical systems (Jefferson et al., 2007). However not all U deposits are associated with graphitic metapelitic gneiss, consideration should be given to the sulphide and mafic mineralogy of basement rock, the activity of Fe^{2+} (Cramer, 1986; Wilde and Wall, 1987; Quirt, 1989; Wilde et al., 1989) and decrease in pH of an alkaline fluid, with iron being the electron acceptor to convert U^{6+} to U^{4+}, heat flow (Hoeve and Quirt, 1984), and electrochemical potential (Jefferson et al., 2007). The basement fluid must also have been alkaline and under saturated in silica to cause the ubiquitous

quartz dissolution above ore deposits (Jefferson et al., 2007). Geophysical, geochemical, and mineralogical studies on the region are continually improving and being reapplied to the region.

1.6.2 Schwartzwalder Deposit, Vein Type

The Schwartzwalder deposit, was the United States largest uranium producing mine until its closure, due to persisting environmental contamination. The deposit is similar to Coles Hill that it is a vein-type deposit but on a much larger scale. The deposit is associated with Laramide age (about 70 Ma) hydrothermal fluid flow, faulting, fracturing, and polymetallic vein formation (Caine et al., 2011; Wallace and Karlson, 1985; Ludwig et al., 1985). It is hosted in tightly folded Paleoproterozoic quartzofeldspathic and calcsilicate metasedimentary and metavolcanic rock "units" common in the central southern Rocky Mountains (Caine et al., 2011). A complex network of Paleoproterozoic and (or) Mesoproterozoic pegmatite dikes also intruded these rocks (Caine et al., 2011).

The mineral deposit comprises a network of fault veins that host brittley deformed oxide, sulfide, and carbonate mineral assemblages. Fault veins are complex brittle structures that are characterized by elements of both veins (mineral filled fractures) and faults that accommodate shearing of rock, producing fault rocks such as clay-rich gouge (Caine et al., 2011). The primary structure that hosts the Schwartzwalder uranium deposit is the Illinois fault zone (Caine et al., 2011). The Illinois fault zone and associated mineralization is localized in a relatively narrow "lithologic transition zone" composed of quartzite and garnet-biotite-gneiss between hornblende gneiss to the west and mica schists to the south (Caine et al., 2011); Wallace and Karlson, 1985). This zone was later referred to as "the Schwartz Trend" (Caine et al., 2011); for example, Norqist, 2001).

Alteration and vein mineralization suggest the uranium was leached from basement rocks, and that brecciation provided conduits for mineralization fluids, and chemical deposition of the uranium. Mineralization included two episodes of alteration and three stages of vein mineralization (Wallace, 1983). Early carbonate- sericite alteration pseudomorphically replaced mafic minerals, whereas the ensuing hematite-adularia episode replaced only the earlier alteration assemblage (Wallace, 1983). Early vein mineralization produced a minor sulfide-adularia-carbonate assemblage (Wallace, 1983). Later vein mineralization generated the uranium ores in two successive stages (Wallace, 1983). Carbonates, sulfides, and adularia filled the

remaining voids (Wallace, 1983). Clastic dikes composed of fault gouge and, locally, ore were injected into new and existing fractures (Wallace, 1983).

Geologic and chemical evidence suggest that virtually all components of the deposit were derived from major hornblende gneiss units and related rocks (Wallace, 1983). The initial fluids were evolved connate/metamorphic water that infiltrated and resided along the extensive fault zones (Wallace, 1983). Complex fault movements in the frontal zone of the eastern Front Range caused the fluids to migrate to the most permeable segments of the fault zones (Wallace, 1983). Heat was supplied by increased crustal heat flow related to igneous activity in the nearby Colorado mineral belt (Wallace, 1983). Temperatures decreased from 225 degrees Celsius to 125 degrees Celsius during later mineralization, and the pressure episodically dropped from 1,000 bars (Wallace, 1983). Sudden decreases in confining pressure during fault movement caused evolution of CO_2 and a consequent increase in pH (Wallace, 1983). Uranium was released with destruction of the uranyl complexes; it was subsequently reduced by aqueous sulfur species, thereby leading to the precipitation of pitchblende (Wallace, 1983).

1.6.3 Olympic Dam, IOGC Type

The Olympic Dam is the world's largest deposit of uranium, and accounts for the major part of Australia's uranium resources, though it is a by-product with copper (World Nuclear Association, 2015). The IOCG deposit occurs within a hematite-rich granite breccia complex in the Gawler Craton that is over lain by 300 meters of flat lying sedimentary rocks (World Nuclear Association, 2015). The central core of the complex is barren hematite quartz breccia, with several localized diatreme structures flanked by zones of intermingled hematite-rich breccias and granite breccias (World Nuclear Association, 2015). The deposit contains iron, copper, uranium, gold, silver, rare earth elements (REEs), and fluorine (World Nuclear Association, 2015). The principle mechanisms which formed the complex are considered to have been hydraulic fracturing, tectonic faulting, chemical corrosion, and gravity collapse (World Nuclear Association, 2015). Much of the brecciation occurred in near surface eruptive environment of a caldera complex during eruptions caused by boiling and explosive interaction of water with magma (World Nuclear Association, 2015).

1.7 Coles Hill Uranium Deposit

The Coles Hill deposit includes the amphibolite-gabbro of the Rich Acres Formations and Leatherwood granite. These host rocks are metasediments of the Fork Mountain Formation, striking NE-SW and dipping about 50° SE (Dahlkamp, 2010).

1.7.1 Host Rock Lithology

The dating of the host rocks suggests that both of these Leatherwood granite types experienced ductile deformation in the vicinity of the fault (Aylor et al., 2014). The Rich Acres amphibolite appears to intrude the gneiss during later mineralization. The mylonitic granite was dated at 442 Ma and the Rich Acres amphibolite and biotite gneiss have U-Pb ages of 430 Ma and 432 Ma, respectively (Tappa et al., 2010, 2014; Aylor et al., 2011) (Aylor et al., 2014). The ore mineralization is found in the Leatherwood and Rich Acres, and therefore both are considered part of the Martinsville Igneous Complex.

1.7.2 Hydrothermal Alteration

Uranium deposition from hydrothermal fluids may have been accompanied by alteration through post magmatic, albitization, and with epigenetic fracture controlled mineralization. The sequence of hydrothermal alteration recorded in the augen gneiss and amphibolite appear to have been initiated contemporaneously with a major cataclastic event. This Na metasomatism alteration and association veining also affect Triassic sediments along the northwest margin of the Danville basin indicating that the age of the alteration sequence is younger than 220 Ma (Jerden, 2001; Manspeizer et al., 1989).

The earliest alteration event involved pervasive Na metasomatism. The event is marked mineralogically by the growth of albite at the expense of potassium feldspar and plagioclase, and the growth of riebeckite at the expense of hornblende (Jerden, 2001). Geochemically potassium is depleted, with enrichment in sodium. Na metasomatism appears to have continued throughout cataclastic deformation along the Triassic border fault (Jerden, 2001). The second alteration of involves the removal of SiO_2 from the ore zones and enrichment along the deposit periphery, marking the silicified cataclastic zone associated with the Chatham Fault (Jerden, 2001). Simultaneous with, or following Na metasomatism the region experienced a multi-stage episode

of chloritization (Jerden, 2001). The first by the direct replacement of biotite, and the second as it fills the fractures associated with uranium ore assemblages (Jerden, 2001). U-mineralization involves three-stages: (1) coffinite-apatite, (2) uraninite-calcite bearing fractures, (3) uraninite-zeolite staining, all of which are associated with a reduction in Fe causing hematite staining (Jerden, 2001). The Fe redox front is marked by a boundary between U(IV) in the reducing zone, and U(VI) in the oxidizing zone (Jerden, 2001). The redox front forms as primary chlorite alters to Fe(III) hydroxides and a Fe rich clay minerals(saprolite) (Jerden, 2001). The rate of the front propagating is thus influenced by the rate of chlorite weathering whereas the propagation of the zone containing secondary U(VI) minerals is determined by the weathering of coffinite-apatite ore (Jerden and Sinha, 2003).

1.7.3 Coles Hill Ore Mineralization

U-ore mineralization is hosted within the igneous Martinsville Complex to the west of the Chatham fault. Primary uranium mineralization is uraninite-pitchblende (UO_2) and coffinite ($USiO_4(OH_4)$) (Jerden, 2001). The deposits are epigenetic and occur in the fractures in highly brecciated and mylonitized quartzo-feldspathic gneiss (Leatherwood) and interlayered amphibolite (Rich Acres).

1.7.3.1 Modes of Mineralization. Jerden (2001) and Halladay (et al., 1982) noted at least three generations of uranium mineralization, not including weathering-related mineralization (Dahlkamp, 2010). The earliest and strongest mineralization (1) comprises of U-rich apatite, coffinite, and minor uraninite/pitchblende associated with albite, chlorite, anatase, and sulfides within breccias and cataclastic rocks (Dahlkamp, 2010). This generation is cut by (2) veinlets of coarse-grained calcite, pitchblende, minor coffinite, Ti oxides (anatase), and traces of sulfides and (3) younger veinlets of pitchblende, coffinite, harmotome, quartz, Ti oxides, and pyrite (Dahlkamp, 2010).

Uranium mineralization is present in two modes, as (a) disseminated impregnation and (b) in veins/ veinlets (Dahlkamp, 2010). Disseminated impregnation type mineralization represents two mineral assemblages that consist of coffinite and minor discrete minute crystals (0.03-0.05 mm in diameter) of oxides often in nearly cubic habit, or as relicts of thereof, disseminated in a ground mass of cataclastic/granulated and brecciated gneisses, mainly augen

gneiss less commonly amphibolite (Dahlkamp, 2010). The mineral assemblage of the disseminated uraniferous apatite-coffinite-uranium-oxide-chlorite association is hosted within the augen gneiss as part of the ground mass (Dahlkamp, 2010). The uranium minerals are found to be erratic, occurring in zones throughout the apatite-chlorite matrix, concentrated in narrow bands or near the border feldspar or lithic clasts (Dahlkamp, 2010). Uranium minerals such as coffinite and uraninite/pitchblende are intergrown with the Ti minerals, and also concentrated near rutile and anatase (Dahlkamp, 2010). Whereas, the mineral assemblage of disseminated pitchblende-calcite association is hosted in amphibolite in which it is distributed similarly to the apatite-coffinite-uranium-U oxide-chlorite assemblage within the matrix of granulated and/or brecciated rock (Dahlkamp, 2010).

Vein-type mineralization postdates the disseminated type and is located along fissures from hairline to several millimeters thick (Dahlkamp, 2010). Two mineral assemblages are associated with this vein type. The pitchblende-calcite association restricted to the amphibolite with pitchblende replacing sphene and rutile, and reacted with Ti to form U-Ti phases in the mineral assemblage, as well as the presence of galena in the pitchblende (Dahlkamp, 2010). Halladay (et al., 1982) notes, colloidal pitchblende along with anatase along the rims of the veinlets, and calcite grains on the interior containing U inclusions (Dahlkamp, 2010). The other mineral assemblages is the pitchblende-zeolite association hosted within the augen gneiss, with pitchblende concentrated up to millimeters in width (Dahlkamp, 2010). Zeolite crystals are present with Fe-Ti oxide and pyrite inclusions, and pitchblende masses have traces of coffinite and/or intergrown magnetite, illiminte or other Ti minerals (Dahlkamp, 2010).

1.7.3.2 Mineralization Paragenesis. The mineralization process is associated with cataclasis and syn-tectonic sodium metasomatism (albite-epidote), chloritization (biotite-chlorite), and hematization (albite-hematite) (Jerden, 2001). The earliest alteration event associated with the fracturing and ductile deformation and metamorphism is pervasive Na-metasomatism that caused albitization of the host plagioclase and K-feldspar to produce rapakivi granite, crystallization of neoblastic albite in the fractures, chloritization of biotite, and local formation of reibeckite from hornblende (Aylor et al., 2014). Albitization was followed by growth of fracture-hosted, euhedral neoblastic apatite. The metasomatized rocks often contain several weight percent P_2O_5 (Aylor et al., 2014). Uranium mineralization is coeval with latter

stages of secondary apatite precipitation. Some uranium mineralization is hosted as U(VI) in secondary apatite, but most occurs as U(IV) in coffinite or nearly amorphous "pitchblende" from uraninite (Aylor et al., 2014).

While metasomatism is pervasive, uranium mineralization at Coles Hill is largely restricted to zones where conditions were favorable for reduction of uranium-bearing fluids to precipitate uraninite and oxidize reduced iron to from hematite (Aylor et al., 2014). The uranium deposits that show the most similarities to Coles Hill include hydrothermal Na-metasomatic deposits and hydrothermal granite deposits, both of which exhibit vein-type morphology (Aylor et al., 2014; Cuney and Kyser, 2008; IAEA, 2009). The Coles Hill mineralization also different from most other uranium deposits because the uranium content is a higher percentage than the thorium content (Aylor et al., 2014). Hydrothermal ore deposits are also associated with hydrothermal healed fractures, igneous intrusions (magmatic), and may be related to Cu porphyry deposits.

1.7.3.3 Structural Controls. The North and South ore bodies are structurally controlled between the Chatham fault to the east and the biotite gneiss (Leatherwood granite intrusive). The U-mineralized pods of the South ore body plunge south at 45° and the myolnite foliation dips 30°SE, and the North ore body is less defined and plunges to the north-east at 12° (Aylor et al., 2014). In the south uranium property, the eastern extent of the mineralization is defined by the intersection of biotite gneiss with the Chatham fault (Aylor et al., 2014). The western extent of the mineralization occurs where the biotite gneiss surfaces (Aylor et al., 2014). The schist is colored red by hematite where exposed on the surface, so the western limit of the uranium is evident by the red soil on color aerial photographs (Aylor et al., 2014). The Coles Hill property appears to be a structural trap between the Chatham fault and biotite gneiss below, with myolnite foliation at 30°SE.

1.7.3.3.1 Fracture Flow & Hydrogeology. The Coles Hill region's modern hydrologic system is structurally controlled. The Chatham fault hydrogeological influence on the ground water system is minimally permeable, and the quantities of flow do not exceed 0.2 m^2/day (Gannon et al., 2012). The fault allows enough flow to preserve the connectivity between the wells as evidence that ground water mixing occurs close to the structure (Gannon et al., 2012). The origin of hydrological recharge remains unknown. Speculations of the nature of flow and

age of the water center on intersecting fractures zones and, brecciated veinlets that have a higher water transsmisivity, as well as the natural hydraulic head.

Jerden (2001) studied the saprolite at Coles Hill and found uranium mineralization associated with apatite and iron oxide, especially in a zone below the water table (Aylor et al., 2014). Within the present hydrologic system that has developed in saprolite, secondary apatite is effective at immobilizing uranium (Jerden, 2001; Aylor et al., 2014).

1.7.3.4 Uranium Ore Potential. Coles Hill deposit is reported to contain over 22,000 metric tons U_3O_8 at an average grade of 0.113 weight percent (Halladay, 1989). The Cole Hill uranium research acquired approximately 20,000 meters of core and percussion cuttings retained by the Virginia Museum of Natural History (VMNH) and the Department of Geological Sciences at Virginia Tech, and augmented by a geochemical investigation of 47 cores samples by the U.S. Geological Survey (USGS) (Jerden, 2001). Although total reserve estimations are significant, the Virginia legislature initiated a ban on uranium mining (Legislative bill number 45.1-283) in 1982. Virginia Uranium Inc. acquired the Coles Hill Uranium Property, and produced a technical report evaluating the economic potential of the North and South ore bodies in 2007.

1.8 Current Research

What was the source of the uranium in the Coles Hill deposit? Did hydrothermal waters moving along the Chatham fault zone transport uranium from the Mesozoic basin into the deformed Martinsville complex and along fractures into a zone of lower Eh and pH where the uranium was deposited (Tappa et al., 2014). While there is no information regarding the presence of uranium bearing clastics in the Danville basin, U-rich sediments, primarily black shales are present in other Mesozoic rift basin of Eastern U.S. (Pratt et al., 1985).

Or was the uranium leached from granite of the Martinsville complex in a manner much like the uranium depletion documented in the Granite Mountains of Wyoming (Rosholt and Bartel, 1969) to be deposited within a reducing zone of fractures. In the case of the Granite Mountains the redeposition occurred at essentially (very nearly) the same time as the removal.

The current research is an attempt to date the fracture controlled uraninite mineralization. If the age determined is Pre-Triassic, then a connection with sediments of the Danville basin is

eliminated. If the age determined is post-Triassic, the result will be that the age of the mineralization will be known, but the source of the uranium is unknown.

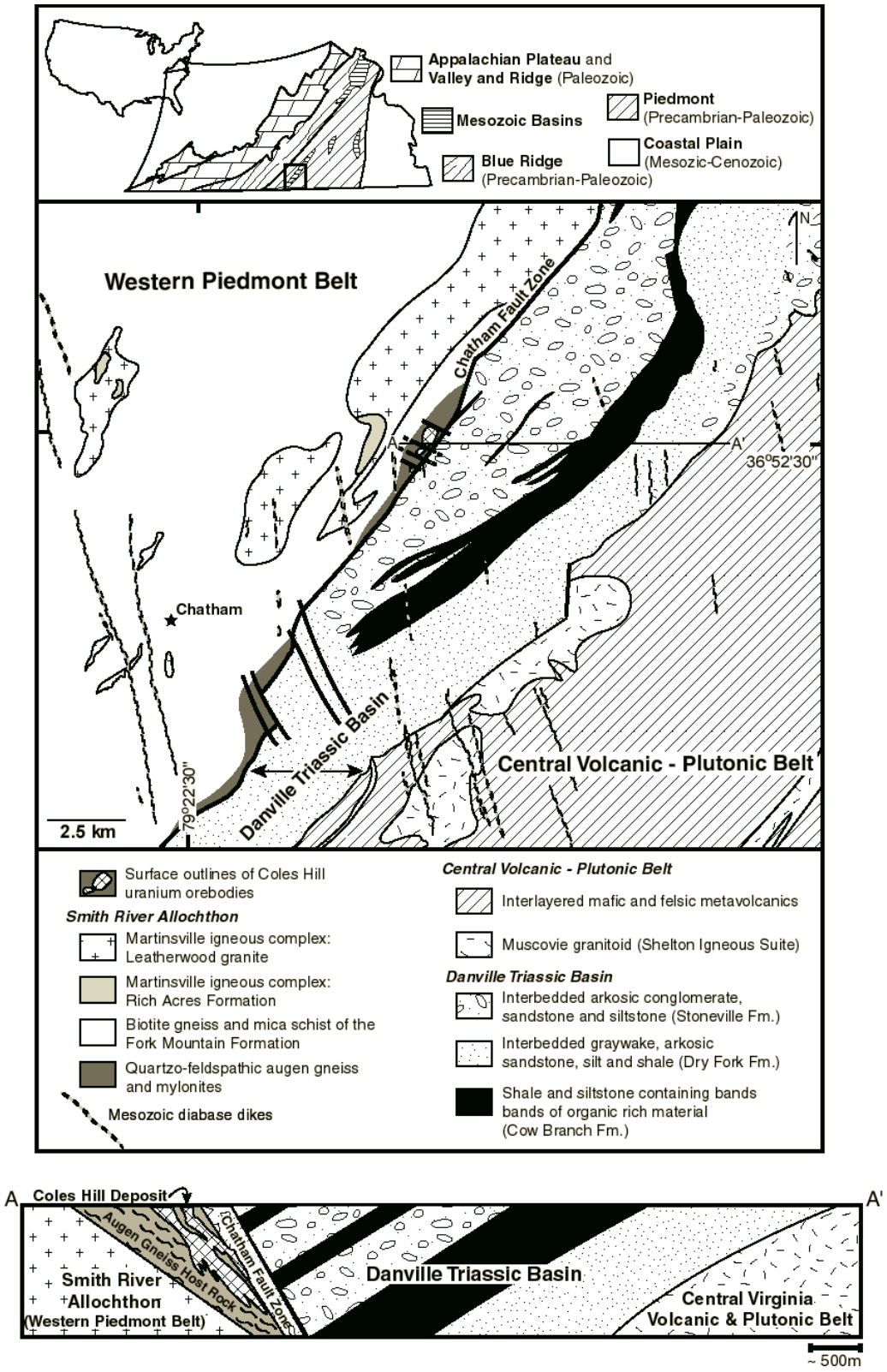

Figure 1.1 Coles Hill regional geologic map and cross section A-A' of ore bodies (From Jerden, 2001). Adapted from Henika, unedited draft (1998).

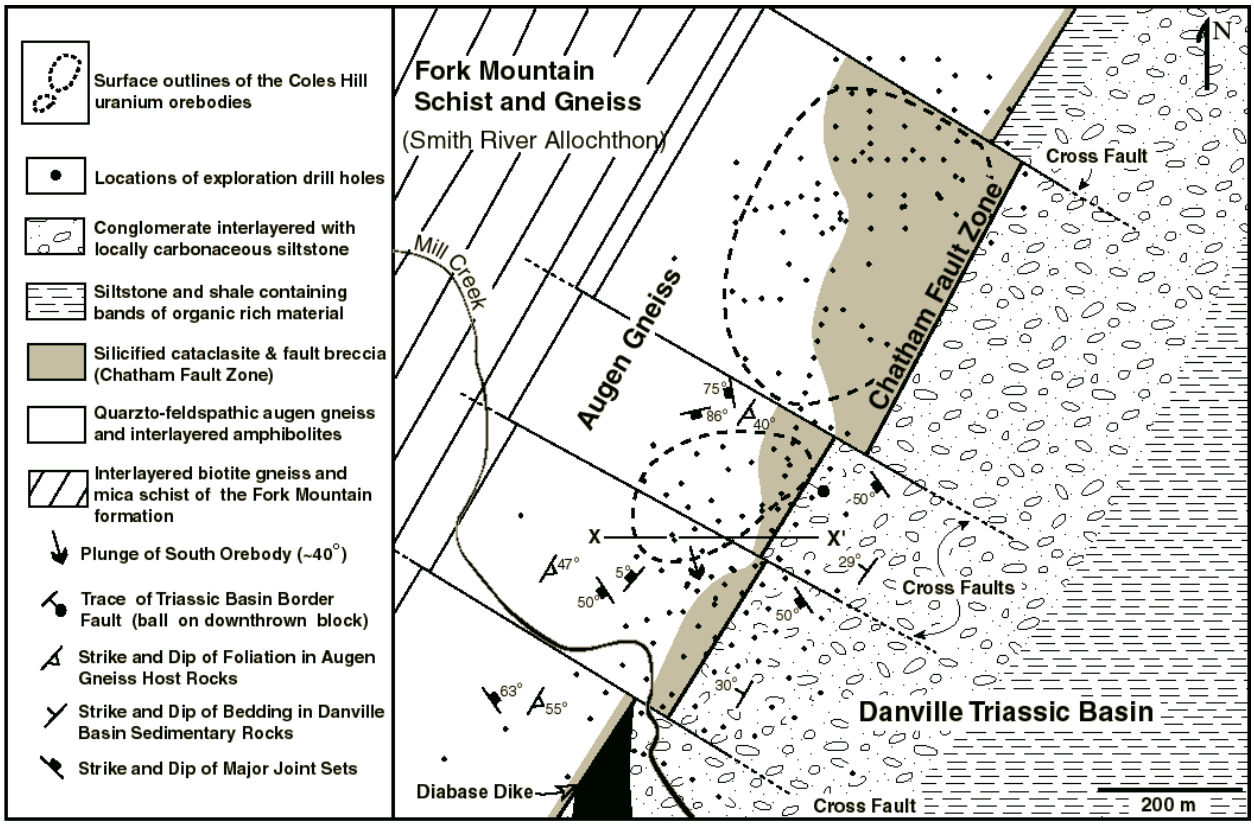

Figure 1.2 Geologic map of Coles Hill site lithological units, and exploration drill hole locations of the south ore body (Marline Corporation, 1983). The geologic map data is from Henika and Thayer (1983), Lineberger (1983), and Jerden (2001).

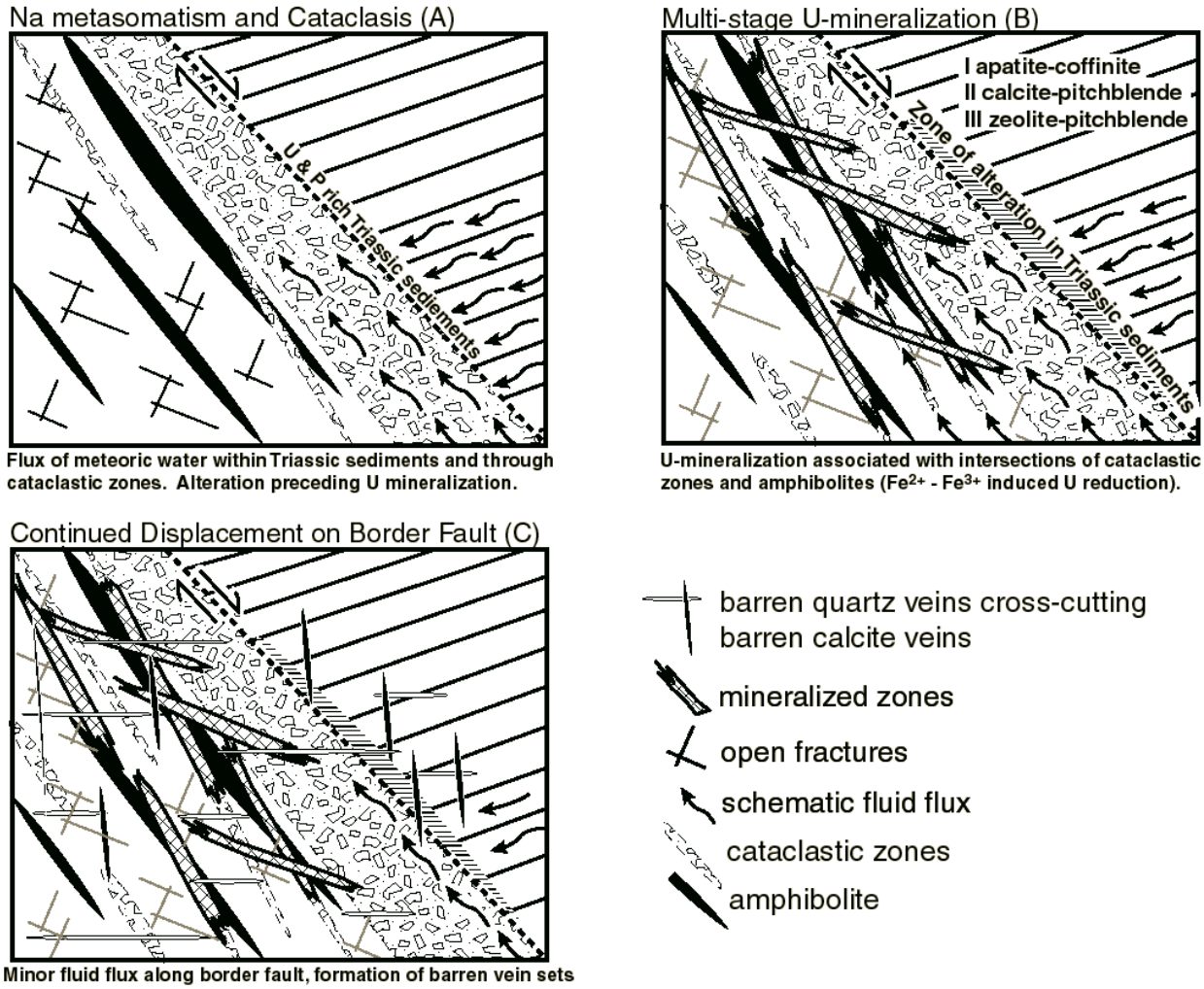

Figure 1.3 Conceptual model for the formation of the Coles Hill uranium deposit. (A) Alteration events by Na-metasomatism and cataclasis along the Chatham fault zone precede U-ore mineralization. (B) Hydrothermal alteration at intersecting cataclastic zones by amphibolite, releases the Fe from mafic minerals, reducing the U in hydrothermal solution, and precipitating ore assemblages. The source of U and P to produce ore assemblages may have been from Triassic Cow Branch Formation, organic rich, fossiliferous shales and mudstones. (C) U-ore assemblages are cross-cut by non-ore bearing quartz and calcite from late stage displacement on the Triassic border fault (Jerden, 2001).

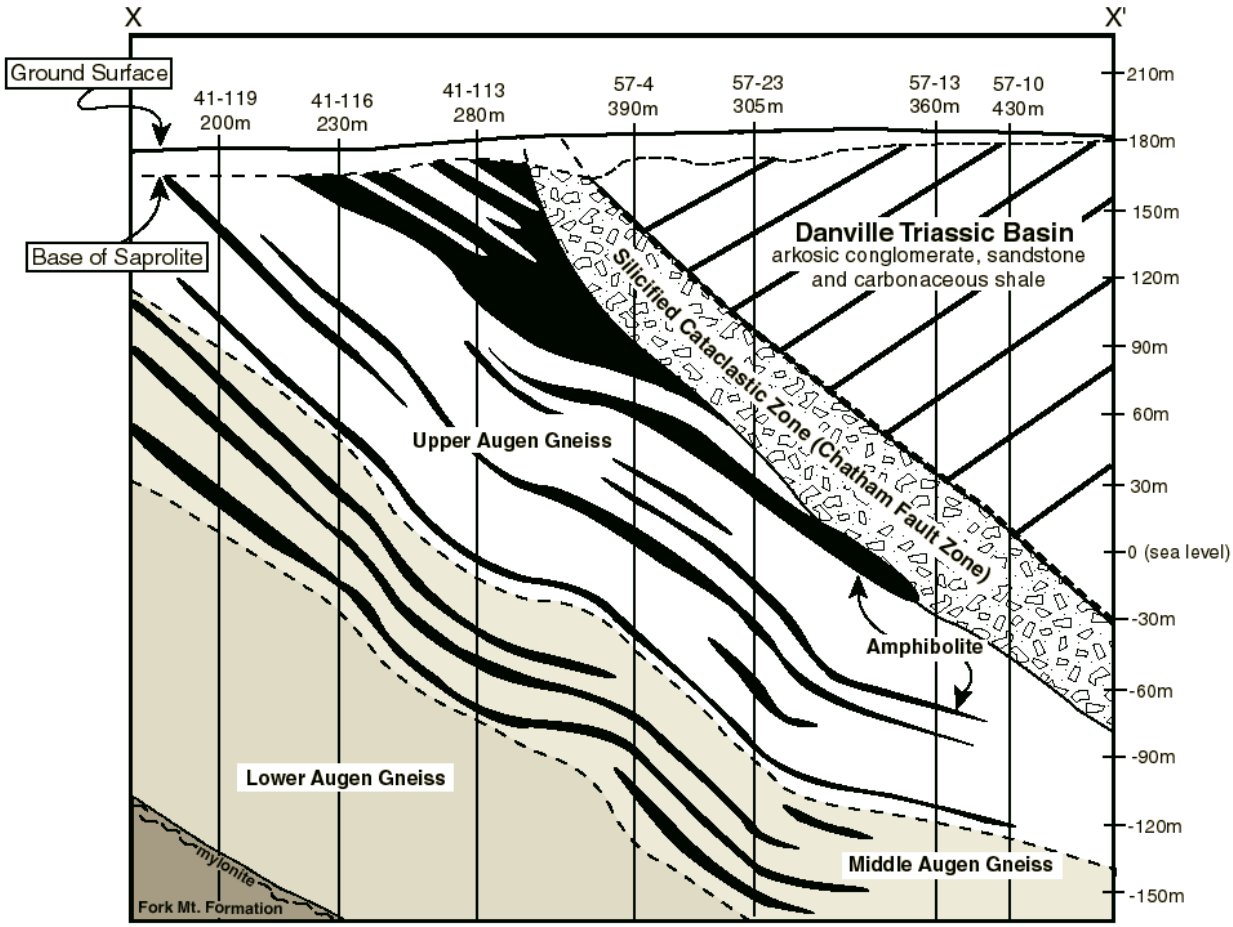

Figure 1.4 Geologic cross-section X-X' of Coles Hill uranium deposit host rocks constructed from Marline Corporation exploration drill hole data (From Jerden, 2001; Marline Corporation, 1983).

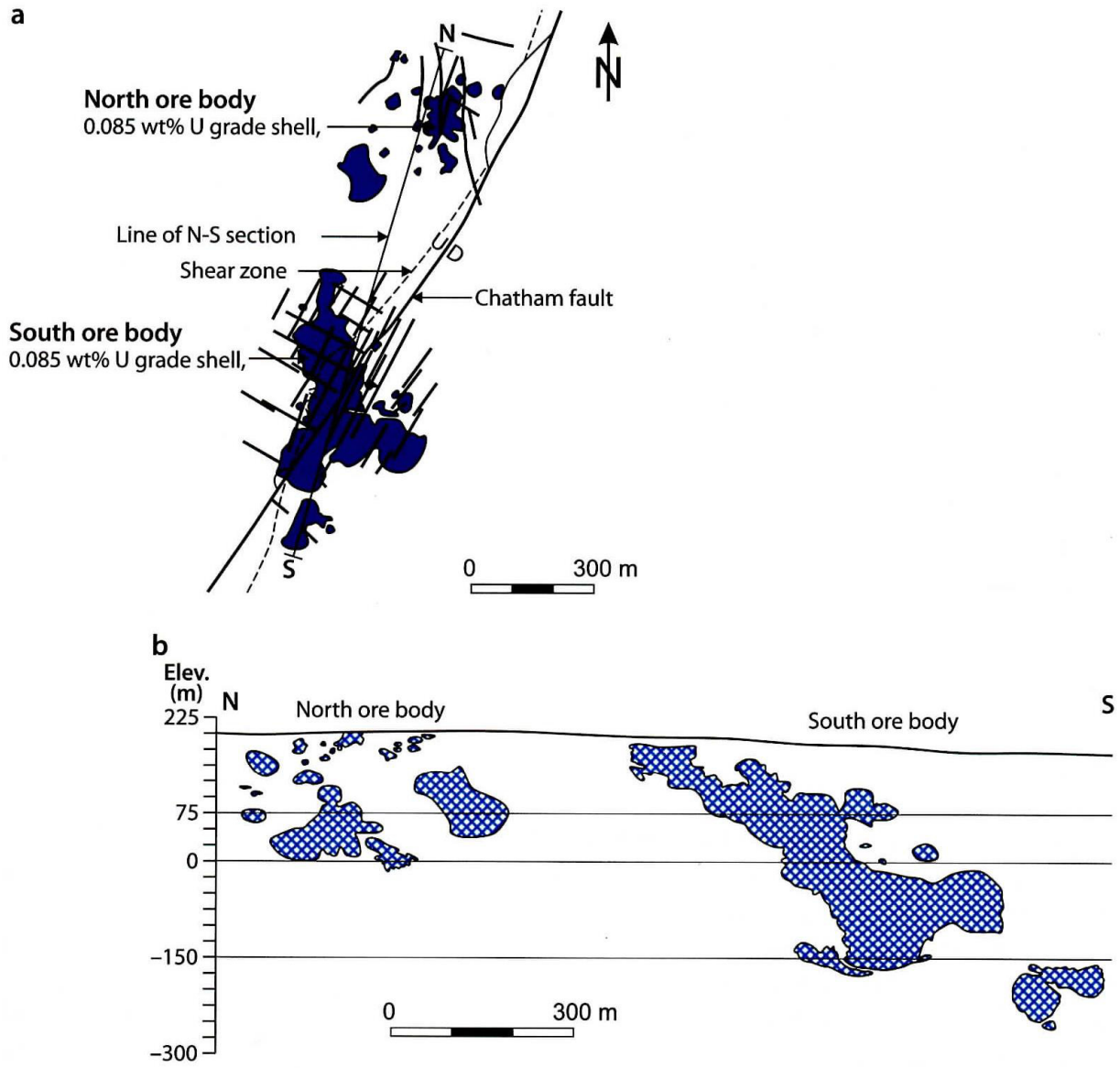

Figure 1.5 Coles Hill deposit, (a) plan view of surface projected ore bodies and (b) S-N outlined by cutoff grade of 0.084% uranium (Dahlkamp, 2010; After Maxwell et al., 2009).

CHAPTER 2

U-PB SYSTEMATICS

2.1 U-Pb Geochronology, Uranium Lead Ratio Systematics

U-Pb geochronology is used to date minerals, such as the pitchblende found at Coles Hill by comparing the ratios of present day radioactive isotopes to their decay products. Two isotopes of U decay to Pb by the following α decay schemes (Steiger and Jager, 1977).

$$^{238}\mathrm{U} \rightarrow 8\ ^{4}\mathrm{He} + {}^{206}\mathrm{Pb} \qquad \lambda_{238} = \left(1.551 \times 10^{-10}\right)\Big/\mathrm{yr.} \qquad \tau_{1/2} = 4.47 \times 10^{9}\ \mathrm{yr.}$$

$$^{235}\mathrm{U} \rightarrow 7\ ^{4}\mathrm{He} + {}^{207}\mathrm{Pb} \qquad \lambda_{235} = \left(9.849 \times 10^{-10}\right)\Big/\mathrm{yr.} \qquad \tau_{1/2} = 0.707 \times 10^{9}\ \mathrm{yr.}$$

2.1.1 Simple Radioactive Isotope Decay

Radioactive decay is the result of an isotope transforming from an unstable parent nuclide to a stable daughter nuclide. Methods used to date uranium bearing minerals rely on the known rate of decay of ^{238}U to ^{206}Pb and ^{235}U to ^{207}Pb. U-Pb dating methods are typically used for minerals that do not contain Pb at the time of formation ("common lead") although there are often ways to correct for initial Pb.

In the simple decay equation where λ is the decay constant,

$$\mathrm{N} = \mathrm{N}_0 \left(e^{-\lambda t}\right)$$

N represents the present day (time *t*) number of atoms of a radioactive nuclide, and N_0 is the number of atoms present at zero time. Since the number of daughter atoms $D^* = N_0 - N$ the equation can be stated as

$$D^* = \mathrm{N}_0 \left(e^{\lambda t} - \mathrm{N}\right)$$

$$D^* = \mathrm{N}\left(e^{\lambda t} - 1\right)$$

The U-Pb decay systems can be represented by the following the decay equations:

$$^{206}\mathrm{Pb} = {}^{238}\mathrm{U}\left(e^{\lambda 8t} - 1\right) \qquad \text{(equation 1)}$$

$$^{207}\mathrm{Pb} = {}^{235}\mathrm{U}\left(e^{\lambda 5t} - 1\right) \qquad \text{(equation 2)}$$

The parent to daughter ratios can be seen by rearranging the following equations:

$$\frac{^{206}\mathrm{Pb}}{^{238}\mathrm{U}} = \left(e^{\lambda 8t} - 1\right)$$

$$\frac{^{207}\mathrm{Pb}}{^{235}\mathrm{U}} = \left(e^{\lambda 5t} - 1\right)$$

The expressions above can be used to calculate the age of uranium bearing minerals in which all the lead is radiogenic and which have remained closed U-Pb systems. Dividing the equation by 2 by equation 1 yields

$$\frac{^{207}\mathrm{Pb}}{^{206}\mathrm{Pb}} = \frac{1}{137.88} \times \frac{\left(e^{\lambda 5t} - 1\right)}{\left(e^{\lambda 8t} - 1\right)} \qquad \text{(equation 3)}$$

Using equation 2 an age can be calculated without knowledge of the uranium concentration of the mineral. The value of 137.88 is the present day ratio of ^{238}U/^{235}U, and λ_8 and λ_5 are the decay constants of ^{238}U and ^{235}U, respectively. Equation 3 is transcendental and best solved by substituting various values for *t* until there is an agreement between the calculation ratio and measured ratio of ^{207}Pb/^{206}Pb.

Decades of experience have shown that in many or most cases ages calculated by the three equations do not agree. Typically the results are that the age calculated from equation 3 is greater than the age calculated from equation 2 which is greater than the age derived from

equation 1. The reason for this discordance is that many uranium bearing minerals commonly do not remain closed systems and this is likely due to the effects of radiation damage. Wetherill (1956) showed that it is often possible to determine the crystallization age of minerals having discordant U-Pb ages.

Figure 2.1 is a graphical interpretation of Wetherill's (1956) calculations. The curve labeled Concordia is the locus of all ratios yielding equal $^{206}Pb^*/^{238}U$ and $^{207}Pb^*/^{235}U$ ages.

Most commonly the discordancy of ages is due to the loss of Pb from minerals. A sample that has undergone Pb loss would plot below Concordia along the chord connecting the age of crystallization to the age of Pb loss as seen in Figure 2.2, this chord is called discordia. Figure 2.3 shows the trajectory for U loss within a system. While Pb loss results in $^{206}Pb^*/^{238}U$ and $^{207}Pb^*/^{235}U$ ratios plotting below Concordia, the same effect is produced by the gain of uranium. In contrast a loss of uranium or gain of lead will result in $^{206}Pb^*/^{238}U$ and $^{207}Pb^*/^{235}U$ ratios plotting above Concordia.

The concordia-discordia method can be used only on minerals that contain no initial Pb or initial Pb in such small quantities that a correction for its presence can be accurately made. Initial or "common" Pb can be detected by the presence of ^{204}Pb. Because in most cases the isotopic composition of common lead cannot be known precisely, such corrections are useful only when the amount of common or initial lead is almost negligible.

For minerals that form with initial lead another approach can be used. The total lead in a sample is equal to the amount of initial lead ($^{207}Pb_0$) plus the radiogenic lead (Pb*) that has accumulated.

$$^{207}\mathrm{Pb} = \left(^{207}\mathrm{Pb}\right)_0 + {}^{207}\mathrm{Pb}^* \qquad \text{(equation 4)}$$

Substituting from equation 1 and rearranging terms

$$^{207}\mathrm{Pb} - \left(^{207}\mathrm{Pb}\right)_0 = {}^{235}\mathrm{U}\left(e^{\lambda_5 t} - 1\right) \qquad \text{(equation 5)}$$

Similarly an expression can be written for total ^{206}Pb

$$^{206}\mathrm{Pb} - \left(^{206}\mathrm{Pb}\right)_0 = {}^{238}\mathrm{U}\left(e^{\lambda_8 t} - 1\right) \qquad \text{(equation 6)}$$

Both sides of equations 5 and 6 can be divided by ^{204}Pb which does not change with time. By convention ^{238}U/^{204}Pb is designated by μ, and the ratio of ^{238}U/^{235}U is constant in the Earth at 137.88 (Steiger and Jager, 1977).

$$\frac{^{207}\text{Pb}}{^{204}\text{Pb}} = \left(\frac{^{207}\text{Pb}}{^{204}\text{Pb}}\right)_0 + \frac{\mu}{137.88}\left(e^{\lambda_5 t} - 1\right) \qquad \text{(equation 7)}$$

$$\frac{^{206}\text{Pb}}{^{204}\text{Pb}} = \left(\frac{^{207}\text{Pb}}{^{204}\text{Pb}}\right)_0 + \mu\left(e^{\lambda_8 t} - 1\right) \qquad \text{(equation 8)}$$

The equations can be rearranged by subtracting the initial value from both sides (White, 2013). The Δ is used to designate the difference between initial and present ratio, therefore the equation becomes:

$$\Delta\frac{^{207}\text{Pb}}{^{204}\text{Pb}} = \frac{\mu}{137.88}\left(e^{\lambda_5 t} - 1\right) \qquad \text{(equation 9)}$$

and

$$\Delta\frac{^{206}\text{Pb}}{^{204}\text{Pb}} = \mu\left(e^{\lambda_8 t} - 1\right) \qquad \text{(equation 10)}$$

Finally by dividing equation 9 by equation 10 yields

$$\frac{\Delta\frac{^{207}\text{Pb}}{^{204}\text{Pb}}}{\Delta\frac{^{206}\text{Pb}}{^{204}\text{Pb}}} = \frac{1}{137.88} \times \frac{e^{\lambda_5 t} - 1}{e^{\lambda_8 t} - 1} \qquad \text{(equation 11)}$$

Equation 11 has been referred to as the Pb-Pb isochron equation. On a plot of ^{206}Pb/^{204}Pb vs ^{207}Pb/^{204}Pb for a series of samples that all stared with the same initial isotopic composition of Pb at some time t_0, and which all remained closed to gain or loss of Pb or U, the measured lead isotope ratios form a linear array whose slope depends on time and three constants (λ_5, λ_8, and

$^{238}U/^{235}U$). The age is derived without knowledge of the parent-daughter ratio. The equation is transcendental and is solved by iterative substitution of various values of *t*.

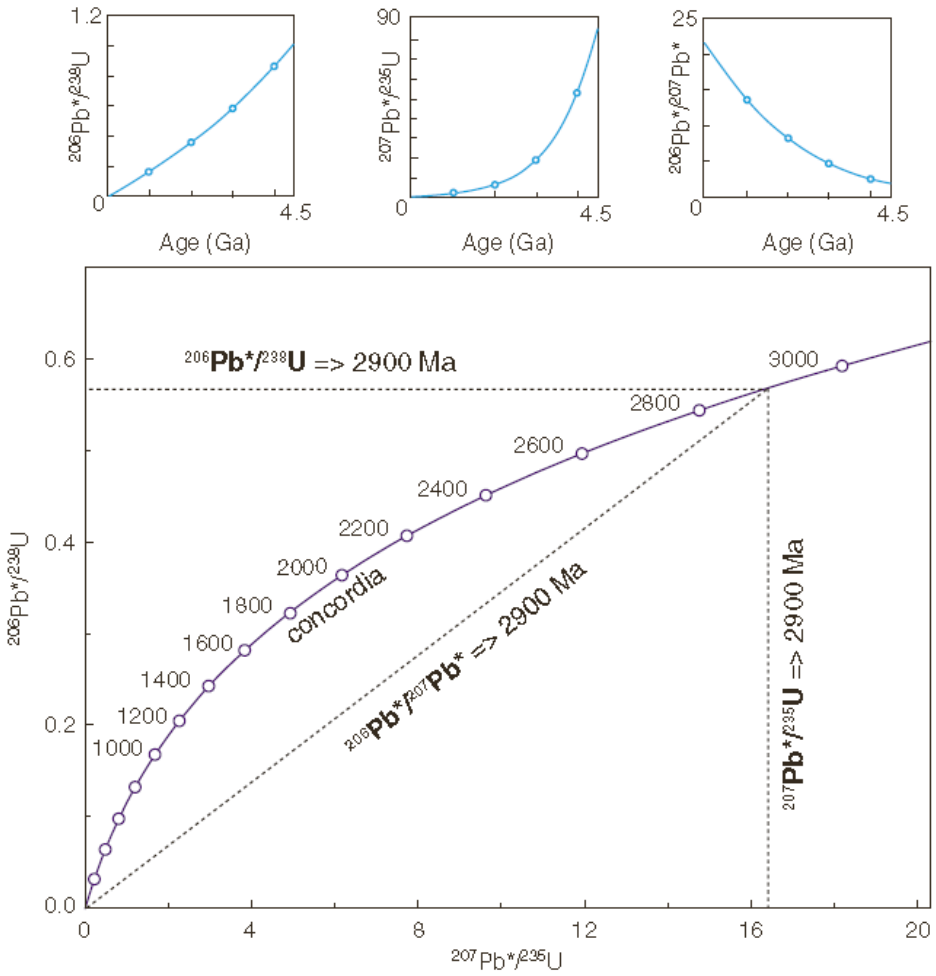

Fig. 2.1 Pb*/U Concordia diagram, showing the three chronometers that are commonly used. The Concordia lines show coincidence of the three chronometers as a function of age (Wetherill, 1956). Figure from Gehrels (2012).

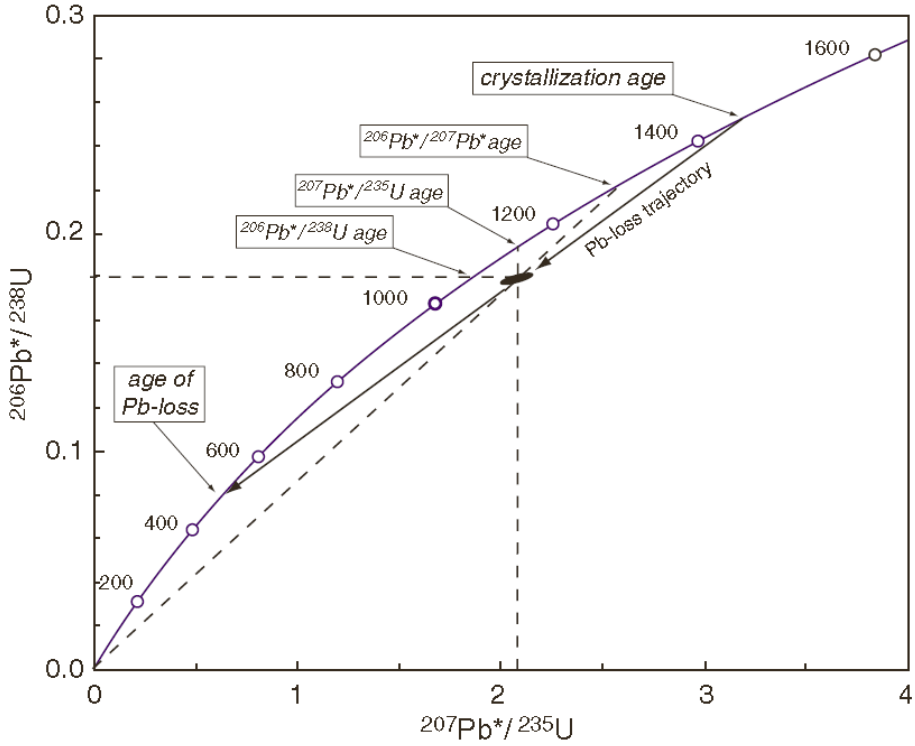

Figure 2.2 Diagram showing that, for a mid-Proterozoic analysis with Pb loss, the $^{206}Pb^*/^{207}Pb$ age is more accurate than $^{206}Pb^*/^{238}U$ and $^{207}Pb^*/^{235}U$ ages. This is why $^{206}Pb^*/^{207}Pb^*$ ages should be used for samples in the ~800-1400 Ma range (assuming that discordance is due to Pb loss), been though $^{206}Pb^*/^{238}U$ ages are generally more precise (Gehrels, 2012).

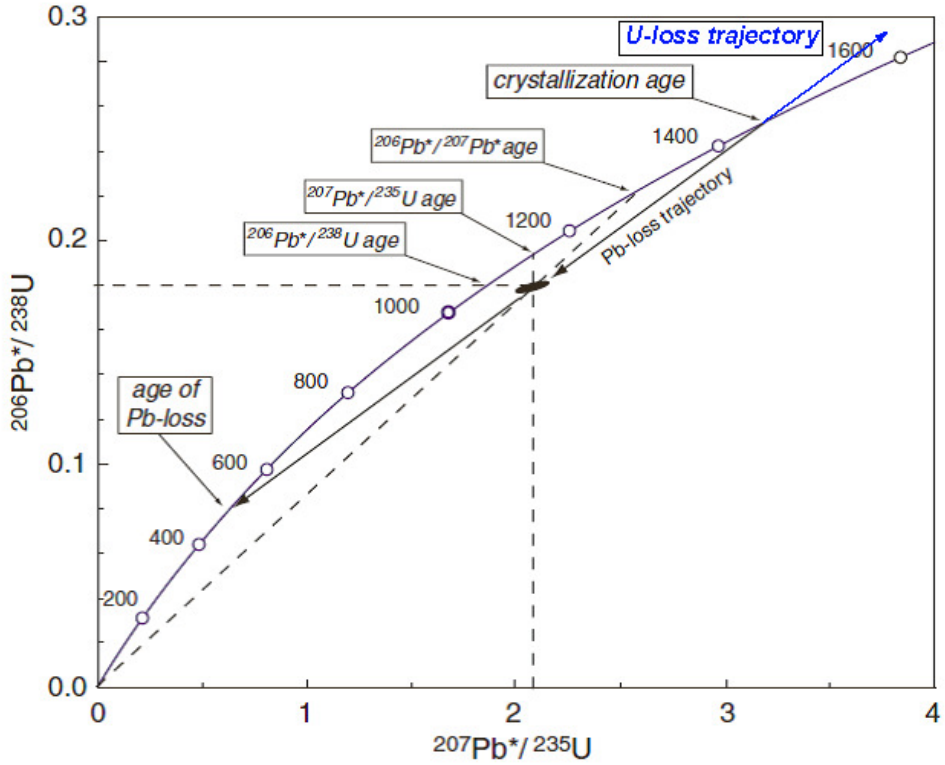

Figure 2.3 Shows the trajectory of a line above Concordia that is representative of U-loss within the system (Adapted from Gehrels, 2012).

CHAPTER 3

METHODS

3.1 Sampling

During the summer, 2014, field observations and sample collection were done with the guidance of Joe Aylor of Virginia Uranium and James Beard of Virginia Museum of Natural History. Using a hand-held gamma ray scintillation counter, samples were taken from Virginia Uranium owned cores that contained fractures that exhibited high activity (gamma).

Pitchblende mineralization occurs along highly complex breccia stockwork fractures only microns wide. Mineralization is accompanied by hematization, or Fe oxidation along the fractures (Iron Redox Zone). Using a dissecting microscope, the pitchblende mineral was separated by hand from the mylonitic Leatherwood granite, and Rich Acres gabbro, along the fractured lustrous black surfaces. Care was taken to avoid the iron oxidation along the edges of fractures. Fifteen samples weighing between 0.037 and 1.64 mg were obtained for analyses.

3.2 Analytical Procedure

Weighed samples were dissolved in pre-cleaned 5 ml Teflon beakers with sub-boiling distilled, 7N nitric acid. After samples were dissolved, they were evaporated to dryness, redissolved, and diluted to 100 ml in 2 percent nitric acid. Samples were split volumetrically into 80 percent and 20 percent aliquots for elemental and isotopic U and Pb analyses respectively. Final dilutions were made when necessary to adjust to concentrations between 10-100 ppb. Elemental analyses were performed with a Thermofischer Element 2 ICP-MS. Pb isotope analyses were determined using a Thermo Neptune, multicollector ICP-MS. Both instruments are housed in the Geochemistry Lab of the National High Magnetic Field Laboratory.

Initial scans of solutions revealed significant amounts of other elements, including Al, Fe, Ca, Si, and Mn, that indicated that the samples dissolved were not pure uraninite.

3.2.1 Pb Isotopic Analyses

Adapted from the procedure of Lugmair and Galer (1992), lead purification was achieved on ion-exchange columns containing anion resin and using a $HBr:HNO_3$ acid as elutant. In this

case, small columns contained 100 micro-liter of anion resin (AG1-X8). Lead collected was dried down, brought back into solution with HBr:HNO_3 and passed again through a fresh resin column. Lead column procedure is detailed in Table 3.1. After the second elution of lead from columns, the samples were evaporated to dryness and then redissolved in 2% HNO_3.

Pb isotope ratios were determined on the multi-collector Neptune ICP-MS, using an Apex Q/Element 2 50 µl nebulizer #1377 for sample injection. Samples were bracketed by NIST-SRM-981 lead isotopic standard during analyses. Two standard deviations of the means of the $^{206}Pb/^{204}Pb$ and $^{207}Pb/^{204}Pb$ for these ten were 0.0038 and 0.0040 respectively.

The Neptune has eight movable Faraday cups and one fixed axial cup. Efficiency of the Faraday cps was calibrated by performing a gain calibration at the beginning of the analyses. The isobaric interference of ^{204}Hg on ^{204}Pb was monitored at mass 202. There was, however, no observable interference on this mass. At the beginning, peak centering was performed and baseline measured by defocusing the beam for 90 seconds while collecting 30 ratios. The Neptune has a 10^{11} Ω resistor, and signal intensities at mass 206 ranged from 2.3 volts to nearly 50 volts. Signal intensities were converted to raw isotope ratios $^{206}Pb/^{204}Pb$, $^{207}Pb/^{204}Pb$, and $^{208}Pb/^{204}Pb$ acquired in one block of 80 cycles with and integration time of 8 second.

3.2.2 U and Pb Analyses

From high purity ICP reagents three mixed U-Pb standard solutions were made. One solution was made to have a U/Pb ratio higher than anticipated in samples, one with lower ratio, and one intermediate. The samples aliquots saved for elemental (U-Pb) analyses were run against these standards. Standards and sample solutions were two percent HNO_3. Analyses were performed with the Thermofischer Element 2 using a PFA 100-1585 250 µl nebulizer for sample injection. Data were obtained by a standard-sample bracketing technique. From the standard-sample bracketing it is determined that the uncertainty of the reported U/Pb ratios is plus or minus four percent. ^{206}Pb abundance in samples ranged from about 3 to 12 micro-grams. Total reagent blanks were less than 1 nanno-gram of ^{206}Pb. No blank corrections were made. Uranium blanks were also insignificant.

Table 3.1 Pb Column Worksheet, provided by Afi Sachi-Kocher.

(Pb only) 100 Microliter Anion Columns (AG1-X8), 100-200 mesh (Pb only)		
Date:	8/20/2015	8/21/2015
Analyst: Lauren Olsen		
Column No. 1-18		
Sample No. 1-18		
Cleaning	**Time (1)**	**Time (2)**
1ml 0.25 N HNO3 (30 drops)	2:45	12:11
0.4ml 0.25 N HNO3 (12)	3:40	12:39
SOLUTION A		
Conditioning		
0.5ml Solution A (15)	4:20	12:59
Sample Processing		
Load Sample 0.5-1ml Sol. A	4:47	1:33
Wash 0.15ml Sol. A (5)	5:00	1:52
Wash 0.15ml Sol. A (5)	5:14	2:01
Wash 0.12ml Sol. A (4)	5:23	2:11
Wash 0.15ml Sol. A (5)	5:34	2:21
SOLUTION B		
Wash 0.2ml Sol. B (6)	5:42	2:32
Collect Pb 0.7ml Sol. B (21)	6:20	3:03

Dry down Pb.
Process it though columns (fresh resin) the 2nd time for purification,
using the same cleaning, contition, and processing procedures.

SOLUTION A: 7 ml H2O + 1 ml 2N HBr + 2 ml 2.5N HNO3
SOLUTION B: 7.85 ml H2O + 0.15 ml 2N HBr + 2 ml 2.5N HNO3

As of: 4/7/04

CHAPTER 4

RESULTS

4.1 Data Results

Table 4.1 shows the results of analyses and reveals the chemical and isotopic complexity of this suite of samples. The measured $^{206}Pb/^{204}Pb$ ratios range from nearly 63 to nearly 2,867 and reveal that half of the samples contain a significant common lead component, and the other half are highly radiogenic. The ages reported are those calculated from equations 1, 2, and 3 following corrections for common lead. It should be pointed out that the exact isotopic composition of common lead in the sample is uncertain. However, the corrected value is relatively insensitive to this uncertainty in the case of the samples that are highly radiogenic, e.g. those having $^{206}Pb/^{204}Pb$ ratios greater than 2,000. Common lead corrections for the least radiogenic samples should be viewed with little confidence. Calculated Pb/U and Pb/Pb ages are highly discordant, ranging from approximately 1 to 3760 Ma.

Figure 4.1 is a plot of all samples. The figure clearly shows a separation between the highly radiogenic samples. Two hypothetical "isochrons" are drawn for reference. The isochron formulation requires that a group of samples with difference U/Pb ratios that formed at the same time incorporating lead with a uniform $^{206}Pb/^{204}Pb$ and that have remained closed systems with respect to U and Pb will form a linear array whose slope is equal to the ($e^{\lambda t}$-1), where "t" is the time of formation. It is obvious that for these samples, one or more of these requirements have not been met. The arrows shown on Figure 4.1 indicate the directions in which samples would be moved in $^{206}Pb/^{204}Pb$ – $^{238}U/^{204}Pb$ space by three difference open system processes: loss of U (gain of U would be in the opposite direction), gain of common lead, and gain of radiogenic lead. It seems worthwhile to treat the two groups (highly radiogenic leads and relatively non radiogenic leads) separately.

Figure 4.2 and 4.3 is a Concordia plot of the seven most radiogenic samples corrected for common lead. These are the samples least affected by common lead corrections. All of these plot on or above Concordia. Within analytical uncertainty, the six of these define a strong trend that extend above Concordia and along a very slightly increasing $^{207}Pb/^{235}U$ ratios. This pattern is strongly suggestive of geologically recent loss of uranium.

The four samples with the highest common lead component are plotted on Figure 4.4. If the best fit line through the data represents or closely approximates a Pb-Pb isochron as defined by equation 11, the calculated age is 1115 Ma. This could well be close to the age of Grenville gneisses that constitute basement rocks in this part of the Appalachian Mountains.

Table 4.1 Sample data from the Element 2 and Neptune measurements.

Sample	Element 2 $^{238}U/^{206}Pb$	Element 2 $^{206}Pb/^{238}U$	Neptune $^{207}Pb/^{206}Pb$	Neptune $^{206}Pb/^{204}Pb$	Age (Ma) $^{206}Pb/^{238}U$	Age (Ma) $^{207}Pb/^{235}U$	Age (Ma) $^{207}Pb/^{206}Pb$
CH1	7.87	0.127	0.05140	2866.61	778	660	268
CH2	9.56	0.105	0.05914	2391.52	648	634	585
CH3	30.64	0.0326	0.06506	580.52	209	264	792
CH5	31.27	0.0320	0.28216	62.67	205	830	3420
CH6	1.64	0.611	0.19333	112.80	3100	2930	2810
CH7	2.61	0.384	0.04407	2560.07	2110	1238	1
CH8	5.40	0.185	0.04345	2602.59	1106	768	1
CH9	1.28	0.783	0.05730	2570.91	3760	2030	57
CH10	3.05	0.328	0.04487	2740.38	1845	1140	1
CH11	2.66	0.376	0.04841	2822.39	2075	1290	127
CH12	10.34	0.0968	0.04149	778.45	602	453	1
CH13	24.39	0.0410	0.16245	155.14	261	670	2520
CH14	62.38	0.0160	0.15671	157.07	103	306	2460
CH15	25.73	0.0389	0.10306	338.22	248	453	1710

Common lead corrections used the following values: $^{207}Pb/^{204}Pb = 15.72$ and $^{206}Pb/^{204}Pb = 18.51$

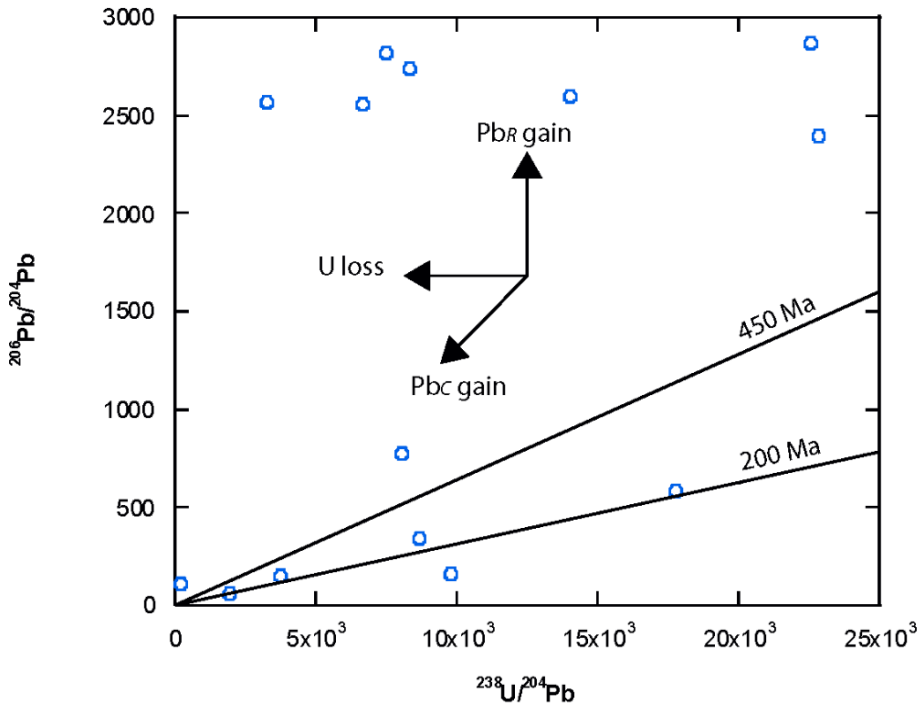

Figure 4.1 U/Pb Isochron shows discordance between samples from Coles Hill. U loss, Pb_R, and Pb_C show three different open system processes. U loss, radiogenic Pb_R gain, and common Pb_C gain in the directions of the arrows away from the U-Pb isochron.

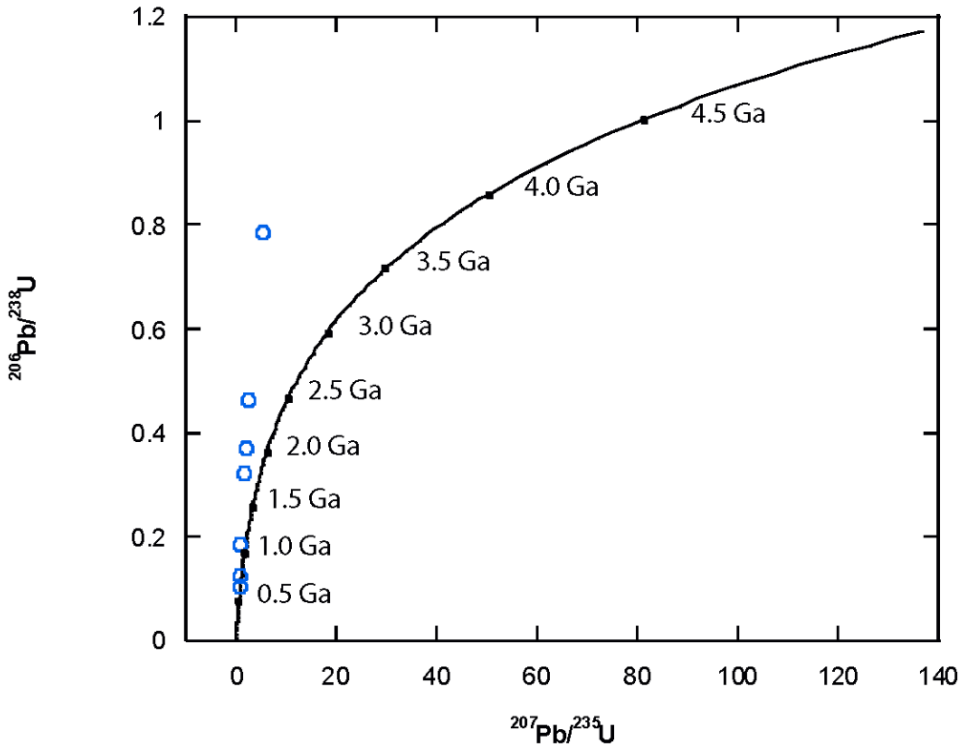

Figure 4.2 U-Pb Concordia plot for the most radiogenic samples corrected for common Pb values. Samples included CH1, CH2, CH7, CH8, CH9, CH10, and CH11, all of which plot on or directly above concordia.

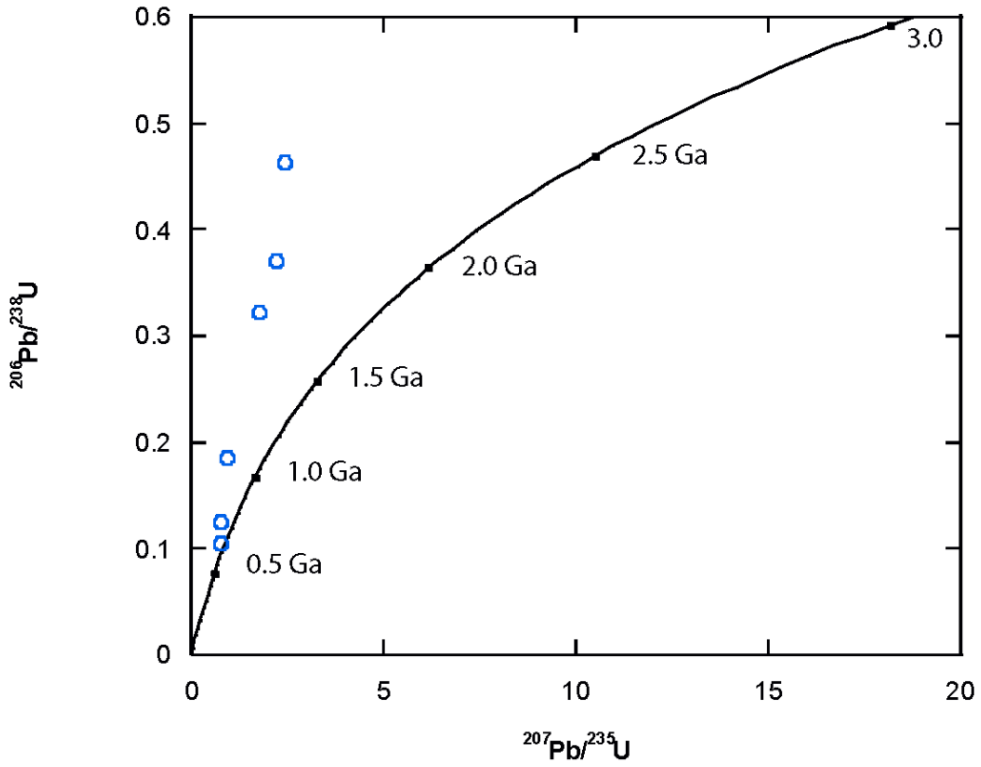

Figure 4.3 Concordia samples with the highest radiogenic values plot above concordia. The data plots away from concordia suggesting evidence of U-loss within the system.

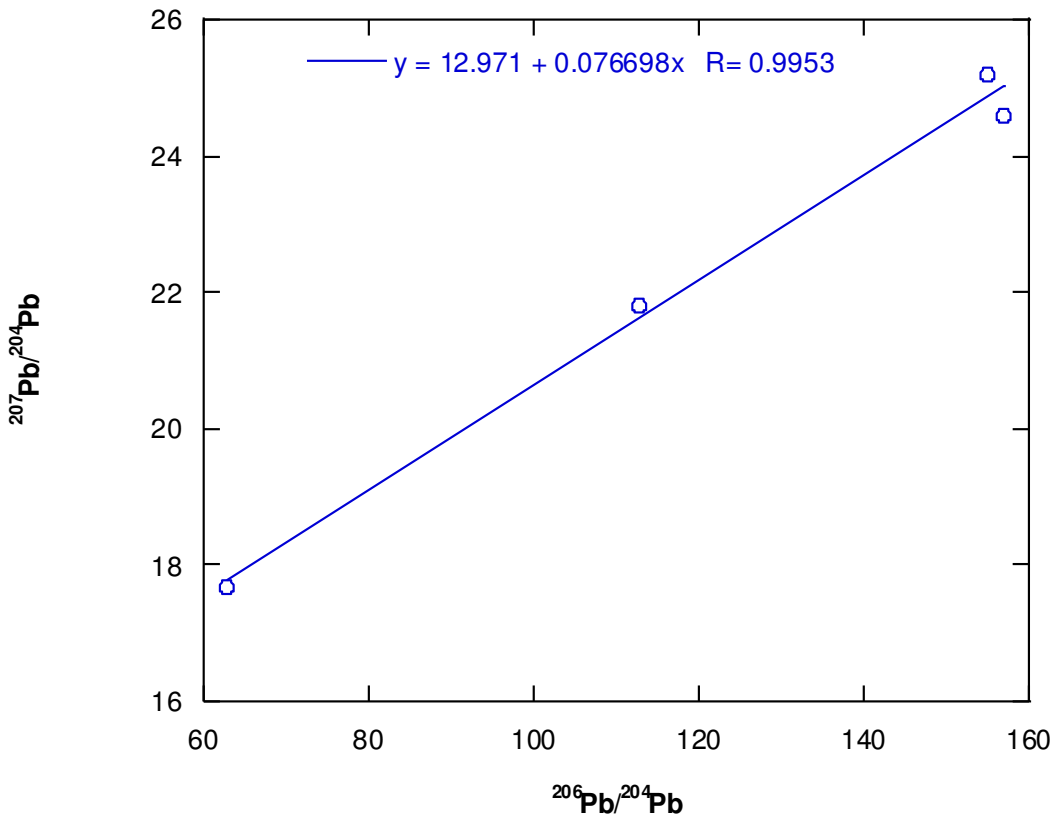

Figure 4.4 Pb/Pb Isochron is a plot of the least radiogenic samples corrected for common Pb values. Samples include CH5, CH6, CH13, and CH14.

CHAPTER 5

DISCUSSION

5.1 Coles Hill Uranium Deposit

The results of analyses presented in Chapter 4 attest to the complexity of the U-Pb systems of these minerals and the processes they have experienced. While the data are not sufficient to determine the age of the Coles Hill uranium deposit, they do allow reasonable inferences to be drawn regarding the systems. Part of the complexity is due to the in homogeneity of the samples on a micron scale. The detection of significant levels of a variety of elements found in the initial ICP-MS scans in this study (see page 35) has been demonstrated by electron microprobe analyses (James Beard, 2015, personal communication) and indicated that the samples are not pure uraninite and coffinite.

Figure 5.1 is an electron backscatter image of a sample of the uranium mineralization provided by James Beard of the Virginia Museum of Natural History. The variable shades of dark grey to white reflect the inhomogeneity. The submicron scale bright spots have been identified as galena (Beard, 2015, personal communication). These small galena crystals might be the source of the large component of common lead present in some of the samples analyzed isotopically. On the other hand, the very old Pb/U ages in Table 4.1(columns 7 and 8) indicate some phase or phases containing significant radiogenic lead that is not supported by uranium. Due to the greater mobility of uranium under oxidizing conditions, uranium could have been lost from samples, while radiogenic lead remained behind to be incorporate in the galena.

That samples plot above the Concordia curve (Figure 4.2), and to the left of the reference U-Pb isochrons of Figure 4.1 is most likely the result of post formation loss of uranium. That the most radiogenic samples do not plot along a single cord indicates that uranium was not lost in a single episode but either as multiple stages or continuously. Where these radiogenic samples plot relative to Concordia and the very young $^{207}Pb/^{206}Pb$ ages (Table 4.1) indicated that uranium loss has been occurring recently (perhaps even today). The soil above the uranium deposits are rich in uranium that is fixed in phosphate minerals (Jerden and Sinha, 2006).

The apparent Pb-Pb isochron date of 1115 Ma suggest the source of this common lead could have been 1110-1200 Ma gneisses that are exposed in the Sauratown Mountains on which the Smith River Allocthon was emplaced.

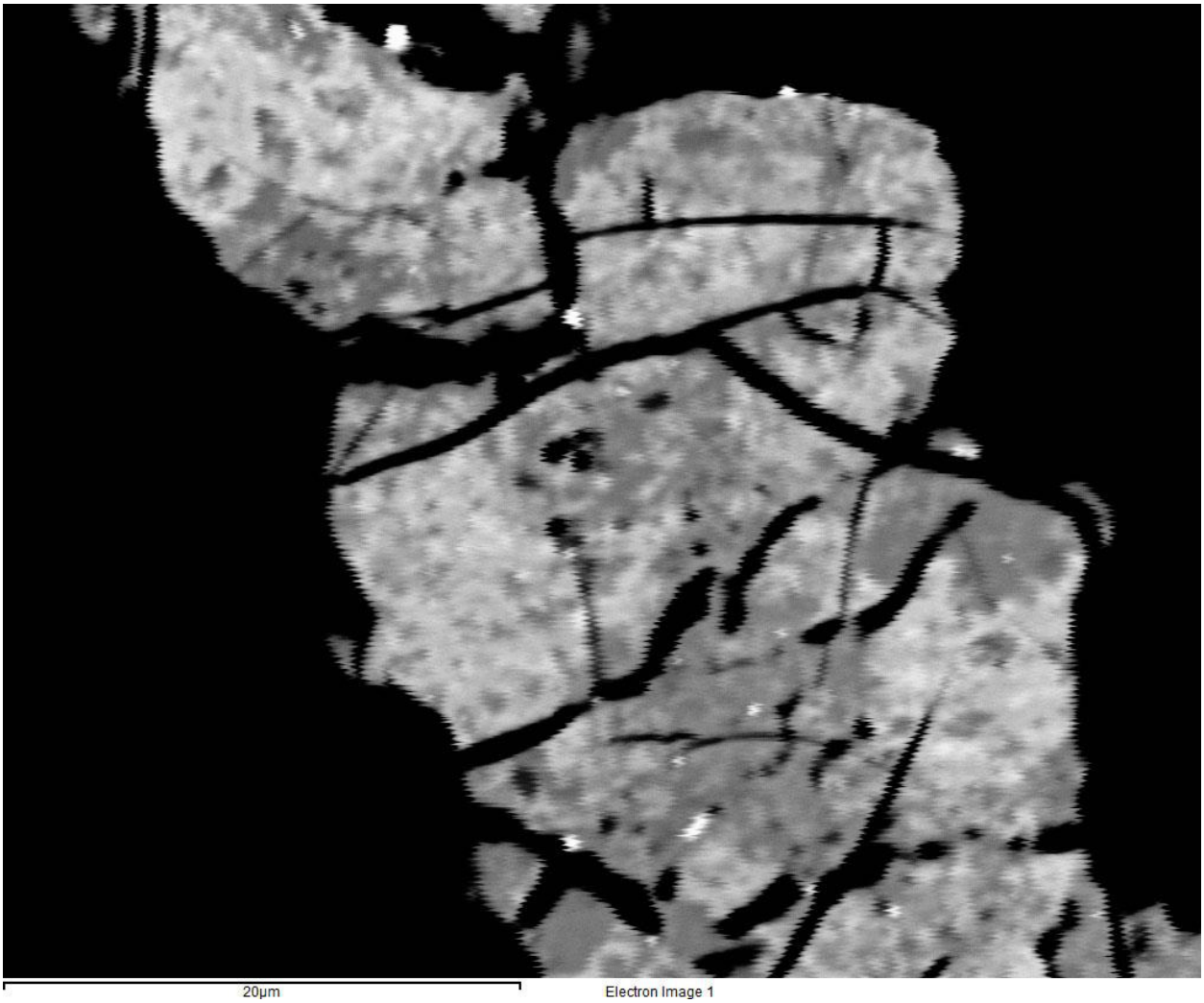

Figure 5.1 Electron Backscatter Image of the UO_2 with micron size galena. Note the bright spots intergrown the size of few microns on the pitchblende. Personal contact with the Virginia Museum of Natural History (Personal communication with Beard, 2015).

REFERENCES

Aylor, J.G., Jr., and Bodnar, R.J., 2010, Current understanding of the Coles Hill uranium deposit, Southside, VA: Geological Society of America Abstracts with Programs, v. 42, no. 1, p. 169.

Aylor, J.G., Jr., Beard, J., Bodnar, R.J., and Tappa, M., 2011, Geology and geochemistry of the Coles Hill uranium deposit. Geological Society of America, Southeastern Section Meeting, March 23-25, 2011, Wilmington, NC, Paper No. 17-3, Abstracts with Programs, v. 43, no. 2, p. 69.

Aylor, J., Jr., Bodnar, R., and Beard, J., 2014, Geology of the Coles Hill uranium deposit, Virginia Piedmont, in Bailey, C.M., and Coiner, L.V., eds., Elevating Geoscience in the Southeastern United States: New Ideas about Old Terranes: Field Guides for the GSA Southeastern Section Meeting, Blacksburg, Virginia, 2014: Geological Society of America Field Guide 35, p. 271–284, doi:10.1130/2014.0035(10).

Beard, J., 2015, Backscatter Electron Image of pitchblende, personal contact, Virginia Museum of Natural History.

Bruneton, P., Cuney, M., Dahlkamp, F, Zaluski, G., 2014, IAEA geological classification of uranium deposits, International Symposium on Uranium Raw Material for the Nuclear Fuel Cycle (URAM 2014), June 2014.

Bruneton, P., International Atomic Energy Agency, 2014, IAEA Classification of Uranium Deposits: http://www-pub.iaea.org/iaeameetings/cn216pn/Monday/Session1/187-Bruneton.pdf (accessed January 2015).

Butler, J.R., and Dunn, D.E., 1968, Geology of the Sauratown Mountains anticlinorium and vicinity, *in* Guidebook for field excursions: Geological Society of America, Southeaster Geology Special Publication 1, p. 19-47.

Caine, J.S., Johnson, R.H., and Wild, E.C., 2011, Review and interpretation of previous work and new data on the hydrogeology of the Schwartzwalder Uranium Mine and vicinity, Jefferson County, Colorado: U.S. Geological Survey Open-File Report 2011–1092, p. 55.

Conley, J.F., 1978, Geology of the Piedmont of Virginia, Interpretations and Problems, *in* Conley, J.F., ed., Contributions to Virginia Geology: Virginia Div. Mineral Resources, Pub. 7, p. 115-149.

Conley, J. F., 1985 Geology of the southwestern Virginia Piedmont: Virginia Div. of Mineral Resources Publication, v. 59, p. 33.

Conley, J.F., and Henika, W.S., 1973, Geology of the snow Creek, Martinsville East, Price and Spray Quadrangles, Virginia: Virginia Div. Mineral Resources Rept. Inv. 33, p. 71.

Conley, J.F., and Henika, W.S., 1973, Fieldtrip across the Blue Ridge Anticlinorium, Smith River Allochthon, and Sauratown Mountains Anticlinorium near Martinsville Virginia, *in* Virginia Minerals: Charlottesville, Virginia, Div. of Mineral Resources, p. 37-44.

Cramer, J.J., 1986, Sandstone-hosted uranium deposits in northern Saskatchewan as natural analogs to nuclear fuel waste disposal vaults: Chemical Geology, v. 55, p. 269-279.

Cuney, M., and Kyser, K., 2008, Recent and Not-So-Recent Developments in Uranium Deposits and Implications for Exploration: Quebec, Mineral Association of Canada, Short Course Series 39, p. 257.

Dahlkamp, F., 2010, Appalachian Highland and Piedmont Region, *in* Uranium deposits of the World: USA and Latin America, Springer, p. 357-366.

Dalrymple, G.B., 1991, Modern Radiometric Methods: How they work, *in* The age of earth, Standford, CA, Stanford University Press, p. 79-124.

Deuzer, W. G., and Herzog, L. F., 1962, Rubidium-strontium age determinations of muscovites and biotites from pegmatites of the Blue Ridge and Piedmont: Journal of Geophysical Research v.67, n. 5, p. 1997-2004.

Fullagar, P.D. and Dietrich, R.V., 1976, Rb-Sr isotopic study of the Lynchburg and probable correlative formation of the Blue Ridge and western Piedmont of Virginia and North Carolina: Am. Jour. Sci, v. 276, p. 346-365.

Fullagar, P.D., and Butler, J.R., 1980, Radiometric dating in Sauratown Mountains area, North Carolina, *in* Price, V., Jr., Thayer, P.A., and Ranson, W.A., editors, Geological investigations of Piedmont and Triassic rocks, central North Carolina and Virginia: Carolina Geological Society Field Trip Guidebook, p. C.G.S. 80 B 11 1-C.G.S. 80 B 11 6.

Gannon, J.P., Burbey, T.J., Bodnar, R.J., and Aylor, J., 2012, Geophysical and geochemical characterization of the ground water system and the role of the Chatham Fault in groundwater movement at the Coles Hill uranium deposits, Virginia, USA. Hydrogeology Journal, v. 20, p. 45-60.

Gates, A.E., 1981, Geology of the western boundary of the Charlotte belt near Brookneal, Virginia (M.S. Thesis): Virginia Polytechnic Institute and State University, Blacksburg, VA, 88 p.

Gates, A.E., 1986, Taconic evolution of the Altavista area, southwest Virginia Piedmont (Ph.D. Dissert.): Virginia Polytechnic Institute and State University Blacksburg, VA, 88 p.

Gates, A.E., Simpson, C., and Glover, L., III, 1986, Appalachian Carboniferous dextral strike-slip faults: an example from Brookneal, Virginia: Tectonics, v. 5, no. 1, p. 119-133.

Gates, A.E., 1987, Transpressional Dome Formation in the southwest Virginia Piedmont: American Journal of Sciences, v. 287, p. 927-949.

Gates, A.E., Lanzirotti, A., and Glover, L., III, 1994, Isotopic evidence for Cambrian tectonics in the crystalline southern Appalachians: the Carolinian, not the Taconian (Abst.): Geological Society of America Abstracts with Programs v. 26, n. 4, p. 15.

Gehrels, G., 2012, Detrital zircon U-Pb geochronology: current methods and new opportunities, *in* Tectonics of Sedimentary Basins: Recent Advances, Blackwell Publishing Ltd, p. 47-62.

Glover, L., III, Speer, J.A., Russell, G.S., and Farrar, S.S., 1983, Ages of regional metamorphism and ductile deformation in the central and southern Appalachians: Lithos, v. 16, p. 223-245.

Halladay, C.R., and Lineberger, H.D., 1982. Geology, Mineralogy and Geophysics of the Coles Hill Uranium deposits, Pittsylvania County, Virginia. For Marline Uranium Corporation. July 1982.

Halladay, C.R., 1989, The Swanson uranium deposit, Virginia: a structurally controlled U-P albite deposit [abs.], in Uranium resources and geology of North America: Saskatoon, Canada, Proceedings of a technical committee meeting organized by the International Atomic Energy Agency, September 1987, p. 519.

Henika, W.S., 1971, Geology of the Basset quadrangle, Virginia: Virginia Division of Mineral Resources Report of Investigations 26, 43 p.

Henika, W.S., 1977. Geology of the Blairs, Mount Hemon, Danville, and Ringgold Quadrangle, Virginia, with sections on the Triassic System by Thayer, P.A. Virginia Division of Mineral Resources Publication 2, 45 p.

Henika, W.S., and Thayer, P.A., 1977, Geologic maps of the Blairs, Mount Hermon, Danville, and Ringgold Quadrangles, Virginia: Virginia Division of Mineral Resources Publication 2, 45 p.

Henika, W.S. and Thayer, P.A., 1983, Geologic map of the Spring Garden quadrangle, Virginia: Virginia Division of Mineral Resources, Publication 48 (GM47D).

Henika, W.S., 1981, Geology of the Spring Garden quadrangle, Virginia: Virginia Division of Mineral Resources Open-File Map and Report, scale 1:24,000.

Henika, W.S., and Thayer, P.A., 1980, Geologic map of the Spring Garden quadrangle, Virginia: Virginia Division of Mineral Resources Publications 48, 1:24,000 scale map with text.

Henika, W.S., 1998, Digital geologic map of the Virginia portion of the Danville 30x60 minute quadrangle: Virginia Division of Mineral Resources Publications DP-43A, unedited draft, scale 1:100,000.

Henika, W.S., Conley, J.F., and Sweet, P.C. 1996, Geology and Mineral Resources of Henry County and the City of Martinsville, Virginia: Charlottesville, Virginia Division of Mineral Resources Publications 137, 22 p.

Hibbard, J.P., Tracy, R.J., and Henika, W.S., 2003, Smith River allochthon: A Southern Appalachian peri-Gondwana terrane emplaced directly on Laurentia: Geology, v. 31, p. 215–218, doi:10.1130/0091 -7613(2003)031<0215:SRAASA>2.0.CO;2.
Hibbard, J.P., Beard, J.S., Henika, W.S., and Horton, J.W., Jr., 2014, The Western Piedmont, in Bailey, C.M., and Berquist, R., eds., The Geology of Virginia: Charlottesville, Virginia, Virginia Department of Mineral Resources, p. 38–73.

Hoeve, J., and Quirt, D.H., 1984, Mineralization and Host Rock Alteration in Relation to Clay Mineral Diagenesis and Evolution of the Middle Proterozoic, Athabasca Basin, northern Saskatchewan, Canada: Saskatchewan Research Council, SRC Technical Report 187, p. 187.

Hoeve, J., and Sibbald, T., 1978, On the genesis of Rabbit Lake and other unconformity-type uranium deposits in northern Saskatchewan, Canada: Economic Geology, v. 73, p. 1450-1473.

IAEA (International Atomic Energy Agency), 2009, World Distribution of Uranium Deposits (UDEPO) with Uranium Deposit Classification: IAEA TECDOC 1629, p. 117.

Jefferson, C.W., Thomas, D.J., Gandhi, S.S., Ramaekers, P., Delaney, G., Brisbin, D., Cutts, C., Quirt, D., Portella, P., and Olson, R.A., 2007, Unconformity associated uranium deposits of the Athabasca Basin, Saskatchewan and Alberta, in Goodfellow, W.D., ed., Mineral Deposits of Canada: A Synthesis of Major Deposit-Types, District Metallogeny, the Evolution of Geological Provinces, and Exploration Methods: Geological Association of Canada, Mineral Deposits Division, Special Publication No. 5, p. 273-305.

Jerden, J.L., 2001. Origin of Uranium Mineralization at Coles Hill Virginia (USA) and its Natural Attenuation within an Oxidizing Rock-Soil-Ground Water System. [Ph.D. thesis]: Dissertation. Dept. Geosci. Virginia Polytechnic Inst. and State Univ. Blacksburg, VA. p. 1-145.

Jerden, J.L., and Sinha, A.K., 2006, Geochemical coupling of uranium and phosphorus in soils overlying an unmined uranium deposits: Coles Hill, Virginia: J. Geochem. Explor., v. 91, p. 56-70.

Jerden, J.L., and Sinha, A.K., 2003, Phosphate based immobilization of uranium in an oxidizing bed aquifer: Applied Geochemistry, v. 13, p. 823-843.

Jonas, A.L., 1927, Geologic reconnaissance in the Piedmont of Virginia: Geological Society of America Bulletin, v. 38, n.4, p. 837-846.

Lehmann, B., 2008, Uranium Ore Deposits: Reviews in Economic Geology, 2, p. 16-24.

Lineberger, D.H., Jr., 1983, Geology of the Chatham fault zone, Pittsylvania County, Virginia: Unpublished M.S. Thesis, University of North Carolina, Chapel Hill, p.79.

Ludwig, K.R., Wallace, A.R., and Simmons, K.R., 1985, The Schwartzwalder uranium deposit—II, Age of uranium mineralization and lead isotope constraints on genesis: Economic Geology and the Bulletin of the Society of Economic Geologists, v. 80, no. 7, p. 1858–1871.

Lugmair G, and Galer, S.J.G., 1992, Age and isotopic relationships among the angrites Lewis Cliff 86010 and Angra dos Reis; Geochim. Cosmochim. Acta, 56 (1992), p. 1673–1694.

Manspeizer, W., DeBoer, J., Costain, J.K., Froelich, A.J., Coruh, C., Olsen, P.E., McHone, G.J., Puffer, J.H., and Prowel, D.C., 1989, Post-Paleozoic activity: in Hatcher, R.D., Thomas, W.A, and Viele, G.W., eds., The Appalachian-Ouachita Orogen in the United States, Geology of North America Volume F-2, Geological Society of America.

McCready, A.J., Annesley, I.R., Parnell, J., and Richardson, L.C., 1999, Uranium-bearing Carbonaceous Matter, McArthur River Uranium Deposit, Saskatchewan, in Summary of Investigations 1999: Saskatchewan Geological Survey, Saskatchewan Energy and Mines, p. 110-120.

Marline Uranium Corporation, 1983, An evaluation of uranium development in Pittsylvania County Virginia: report submitted jointly by Marline Uranium Corporation and Union Carbide Corporation to the Virginia Uranium Administrative Group to the Virginia Uranium Administrative Group Pursuant to Section 45.10285.1et seq of the Code of Virginia (1983) (Senate Bill 155), October, 15, 1983.

Maxwell, R.D., Gibbs, B.L., Pool, T.C., Keim, K.S., Christopher, P.A., 2008, Technical Report on the Coles Hill Uranium Property, Pittsylvania County, Virginia United States of America.

Mueller, P., and Vervoort, J., 2014, Thermal Ionization Mass Spectrometry (TIMS): http://serc.carleton.edu/research_education/geochemsheets/techniques/TIMS.html (accessed June 2015).

Myertons, C.T., 1963, Triassic formations of the Danville basin: Virginia division of Mineral Resources Report of Investigations 6, 65 p.

Nelson, S.A., Tulane University, 2006, Radiometric Dating: http://www.tulane.edu/~sanelson/eens211/radiometric_dating.htm (accessed June 2015).

Norquist, B., 2001, Shrinkage stopping practices at the Schwartzwalder Mine, in Hustrulid, W.A., and Bullock, R.L., eds., Underground mining methods—Engineering fundamentals and international case studies: Society for Mining, Metallurgy, and Exploration, p. 195–204.

Odom, A.L., and G.S. Russell, 1975, The time of regional metamorphism of the Inner Piedmont, North Caroline, and Smith River Allocthon: Inferences from whole-rock ages: Geol. Soc. America Abs. with Programs, v. 7, no. 4, p. 522.

Pratt, L.M., Vuletich, A.K, and Daws, T.A., 1985, Geochemical and isotopic characterization of organic matter in rocks of Newark Supergroup. In: G.R. Robinson, Jr., and A.J. Foelich

(Editors), Proceedings of the Second USGS Workshop on the Early Mesozoic Basins of the Eastern United Sates, U.S. Geol. Surv., Circ., v. 946, p. 74-78.

Price, V., Conley, J.F., Piepul, R.G., Robinson, G. R., Thayer, P.A., and Henika, W.S., 1980, Geology of the Whitmell and Brosville quadrangles, Virginia: Virginia Div. Mineral Resources, Publication. 21 (GM 16 A,D), 1:24,000 scale map with text.

Price, Van, Conley, J.F., Piepul, R.G. Robinson, G.R., and Thayer, P.L., 1980, Geology of the Axton and Northeast Eden quadrangles, Virginia: Virginia Division of Mineral Resources Publication 22 (GM 16 B,C), 1:24,000 scale map with text.

Quirt, D.H., 1989, Host-Rock Alteration at Eagle Point South: Saskatchewan Research Council, Publication No. R-855-1-E-89, p. 95.

Ragland, P.C., 1974, Geochemical evidence for the existence of two igneous rock series, Martinsville Igneous Complex (Abst.): Geological Society of America Abstracts with Programs, v. 6, n. 4, p. 390.

Ramsey, J.C., 1967, Folding and fracturing of rocks: McGraw-Hill Book Company Publishers, New York, NY, 568 p.

Rankin, D.W., 1975, The continental margin of eastern North America in the Southern Appalachians, the opening and clothing of the Proto-Atlantic Ocean, *in* Orville, P.M., and Ostrom, J.H., eds., Tectonics and Mountain Ranges: Am. Jour. Sci. v. 237-A, p. 298-336.

Robinson, G.R., Jr., 1979, Pegmatite cutting myolnite; evidence supporting pre-Triassic faulting along western border of the Danville Triassic basin, southern Virginia (Abst.): Geological Society of America Abstracts with Programs, v. 11, n. 4, p. 210.

Rosholt, J.N. and Bartel, A.J., 1969, Uranium, thorium, and lead systematics of the Granite Mountains, Wyoming, v. 7, p. 141-147. Doi: 10.1016/0012-821X(69)90028-4.

Salters, V.J.M., 2014, Geochemistry Facilities: https://nationalmaglab.org/research/research-groups/geochemistry/facilities, (accessed June 2015).

Sinha, A.K., Hund, E.A., and Hogan, J.P., 1989, Paleozoic accretionary history of the North American plate margin (central and southern Appalachians): constraints from age, origin, and distribution of granitic rocks, *in* Hillhouse, J.W., editor, Deep structure and post kinematics of accreted terrains: International Union of Geology and Geophysics and the American Geophysical Union, Geophysical Monograph 50, p. 219-238.

Standard Reference Material 981 Common Pb Isotopic Standard, NBS-SRM981, 1968.

Stieff, L.R., Stern, T.W., Oshiro, S., and Senftle, F.E., 1959, Tables for the calculation of lead isotopes ages: USGS Professional paper 334-A.

Steiger, R. H. and Jager, E. (1977). Subcommission on geochronology: Convention on the use of decay constants in geo- and cosmochronology. Earth and Planetary Science Letters 36(3): 359-362.

Tappa, M.J., Bodnar, R.J., Ayuso, R.A., Aylor, J.G., Jr., Wooden, J.L., and Vazquez, J.A., 2010, Zircon U/Pb geochronology of host rock and mineralization at the Coles Hill uranium deposit: Geological Society of America Abstracts with Programs, v. 42, no. 5, p. 539.

Tappa, M.J., Ayuso, R.A., Bodnar, R.J., Aylor, J.G., Beard, J., Henika, W.S., Vazquez, J.A., and Wooden, J.L., 2014, Age of host rocks at the Coles Hill Uranium Deposit Pittsylvania County, Virginia, Based on Zircon U-Pb Geochronology. Economic Geology, 109: 515-530.

Tullis, Jan, and Lund, R.A., 1987, Transition from clastic flow to dislocation creep of feldspar: mechanisms and micro structures: Geology, v. 15, p. 606-609.

Wallace, A. R., 1983, Alteration and vein mineralization, Schwartzwalder uranium deposit, Front Range, Colorado: U.S. Geologic Survey Open-File Report: 83-417.

Wallace, A.R., and Karlson, R.C., 1985, The Schwartzwalder uranium deposit—I, Geology and structural controls on mineralization: Economic Geology and the Bulletin of the Society of Economic Geologists, v. 80, no. 7, p. 1842–1857.

Wetherill, G.W., 1956, Discordant uranium-lead ages, *in* Trans. Amer. Geophys. Union, v. 37, p. 320-327.

White, W.M, 2013, Radiogenic Isotope Geochemistry, *in* Geochemistry, John-Hopkins University Press, Wiley Blackwell, URL: http://archive.is/TZCMa#selection-241.50-241.89.

Wilde, A.R., and Wall, V.J., 1987, Geology of the Nabarlek uranium deposit, Northern Territory, Australia: Economic Geology, v. 82, p. 1152-1168.

Wilde, A.R., Mernach, T.P. Bloom, M.S., and Hoffman, C.F., 1989, Fluid inclusion evidence on the origin of some Australian unconformity-associated uranium deposits: Economic Geology, v. 84, p. 1627-1642.

Wilson, N.S.F., Stasiuk, L.D., and Fowler, M.G., 2007, Origin of organic matter in the Proterozoic Athabasca Basin of Saskatchewan and Alberta, and significance to unconformity-associated uranium deposits, in Jefferson, C.W., and Delaney, G., eds., EXTECH IV: Geology and Uranium EXploration TECHnology of the Proterozoic Athabasca Basin, Saskatchewan and Alberta: Geological Survey of Canada, Bulletin 588, (also Geological Association of Canada, Mineral Deposits Division, Special Publication 4; Saskatchewan Geological Society, Special Publication 18) p. 325-340.

World Nuclear Association, 2015, Geology of Uranium Deposits: http://www.world-nuclear.org/information-library/nuclear-fuel-cycle/uranium-resources/geology-of-uranium-deposits.aspx (accessed February 2016).

BIOGRAPHICAL SKETCH

Lauren R. Olsen

Lauren Reneé Olsen was born on January 25, 1990 and grew up in Stuart, Florida. The small city of Stuart located on the inter-coastal waterway allowed her to develop a passion for the ecosystems and marine environments. Her interests and hobbies included all types of outdoor activities, watersports, fishing, scuba, recreational boating, and environmental conservation.

While attending Martin County High School, Lauren spent her summers working as a camp counselor for the Environmental Studies Center located in Jensen Beach, Florida. The day camp focused on providing a safe and fun environment while educating the campers about the local marine ecosystems, the organisms within them, and how to protect them for future generations. Upon graduation she was accepted to the Florida State University in 2008.

Lauren chose to pursue a Bachelor's of Science degree in Geography, more specifically focusing on Environmental Studies. She became passionate about geology during her time spent at FSU; however, budget-cuts and department-cuts prevented her from perusing a geology degree. Her focus on environmental studies allowed her to explore her passion for geology. The summer of 2011 she received an internship with Florida South Eastern Department of Environmental Protection. As an intern she worked with a professional geologist on the Waste Clean-up Section: Closed-Loop Aero-jet Canal Remediation Projected extension of the C-111 Spreader Canal in concordance with the Everglades Restoration Project. The project was led by the South Florida Water Management District, under the supervision of the Department, and along with the Comprehensive Everglades Restoration Program.

In 2012 she graduated from the Florida State University with her Bachelor's degree, and attended FSU's Department of Geology Field Camp in Taos, New Mexico. After spending 6 weeks at field camp, she was certain she wanted to pursue a Master's of Science degree in Geology. Lauren was accepted to FSU's graduate school in 2013, where she would pursue a Master's degree in Geology as part of the Department of Earth Ocean and Atmospheric Science. Upon returning to the university, she was offered a research and teaching assistantship within the program under Dr. Leroy Odom. She would complete her graduate research under his guidance and with the help from others. The first year of working alongside Dr. Odom, Lauren directed

her interests towards economic geology. The Coles Hill Uranium Ore Deposit provided an opportunity for a thesis project by utilizing geochronology to date the pitchblende uranium mineral. The U-Pb geochemical analyses was completed at the NHFML in Tallahassee, Florida. Lauren will complete her Master's degree with honors in spring of 2016, and looks forward to pursuing a career in the mining industry for resource development in the U.S. and abroad.